HHS Public Access

Author manuscript

Nat Neurosci. Author manuscript; available in PMC 2021 December 29.

Published in final edited form as:

Nat Neurosci. 2021 May ; 24(5): 685–693. doi:10.1038/s41593-021-00819-3.

An inhibitory hippocampal–thalamic pathway modulates remote memory retrieval

Gisella Vetere[1,2,8], **Frances Xia**[1,3,8], **Adam I. Ramsaran**[1,4], **Lina M. Tran**[1,3], **Sheena A. Josselyn**[1,3,4,5,6], **Paul W. Frankland**[1,3,4,5,7,✉]

[1]Program in Neurosciences & Mental Health, Hospital for Sick Children, Toronto, Ontario, Canada

[2]Team Cerebral Codes and Circuits Connectivity (C4), Plasticité du Cerveau, ESPCI Paris, CNRS, PSL University, Paris, France

[3]Department of Physiology, University of Toronto, Toronto, Ontario, Canada

[4]Department of Psychology, University of Toronto, Toronto, Ontario, Canada

[5]Institute of Medical Sciences, University of Toronto, Toronto, Ontario, Canada

[6]Brain, Mind & Consciousness Program, Canadian Institute for Advanced Research, Toronto, Ontario, Canada

[7]Child & Brain Development Program, Canadian Institute for Advanced Research, Toronto, Ontario, Canada

[8]These authors contributed equally: Gisella Vetere, Frances Xia

Abstract

Memories are supported by distributed hippocampal–thalamic–cortical networks, but the brain regions that contribute to network activity may vary with memory age. This process of reorganization is referred to as systems consolidation, and previous studies have examined the relationship between the activation of different hippocampal, thalamic, and cortical brain regions

✉**Correspondence and requests for materials** should be addressed to P.W.F. paul.frankland@sickkids.ca.

Author contributions

G.V., F.X., A.I.R., L.M.T., S.A.J. and P.W.F. designed the experiments. G.V., F.X., A.I.R. and L.M.T. conducted the histology and behavioral experiments, and associated data analysis. A.I.R. and L.M.T. performed an independent replication of the main behavioral experiment. P.W.F., F.X., G.V., A.I.R. and L.M.T. wrote and edited the manuscript.

competing interests

The authors declare no competing interests.

Additional information

Extended data is available for this paper at https://doi.org/10.1038/s41593-021-00819-3.

Supplementary information The online version contains supplementary material available at https://doi.org/10.1038/s41593-021-00819-3.

Peer review information *Nature Neuroscience* thanks Magdalena Sauvage, Seralynne Vann and the other, anonymous, reviewer(s) for their contribution to the peer review of this work.

online content

Any methods, additional references, Nature Research reporting summaries, source data, extended data, supplementary information, acknowledgements, peer review information; details of author contributions and competing interests; and statements of data and code availability are available at https://doi.org/10.1038/s41593-021-00819-3.

and memory age at the time of recall. While the activation of some brain regions increases with memory age, other regions become less active. In mice, here we show that the active disengagement of one such brain region, the anterodorsal thalamic nucleus, is necessary for recall at remote time-points and, in addition, which projection(s) mediate such inhibition. Specifically, we identified a sparse inhibitory projection from CA3 to the anterodorsal thalamic nucleus that becomes more active during systems consolidation, such that it is necessary for contextual fear memory retrieval at remote, but not recent, time-points post-learning.

While memories for events may initially depend upon the hippocampus, with time these memories become increasingly dependent upon the cortex for their expression[1–4]. Post-learning communication between the hippocampus and cortex, via the thalamus, is thought to drive this time-dependent reorganization process called systems consolidation[2,5–12]. While the contributions of hippocampal and cortical regions have been studied in detail, much less is known about how thalamic regions contribute to this memory reorganization process at different post-encoding delays.

Using brainwide mapping of immediate early gene induction, we previously identified networks of regions activated by recall of either recent or remote contextual fear memory[11,13]. Thalamic regions played central roles within these networks, with their retrieval-induced activation generally correlated with activity in cortical and hippocampal regions at both retention delays. However, one region, the anterodorsal thalamic nucleus (ADn), exhibited a distinct pattern. Following recall of recent contextual fear memory, ADn activity was positively correlated with activity in other regions, including cortical and hippocampal subregions (Extended Data Fig. 1a). In contrast, at the remote time-point, this pattern switched. Following recall of remote contextual fear memory, ADn activity was negatively correlated with activity in other regions, including cortical and hippocampal subregions (Extended Data Fig. 1b). The ADn has extensive connections with both the hippocampus and the cortex[14–16], and lesioning or inhibiting ADn impairs performance in hippocampus-dependent memory tasks[17–22]. Furthermore, ADn activity is tightly coupled with hippocampal oscillations that play important roles in memory processing[23]. In the network analysis[11,13], the inverse correlation between ADn and other brain regions during remote memory recall raises an intriguing possibility. As other brain regions become more engaged during remote memory recall, ADn activity is actively inhibited by one or more brain regions, and such inhibition may be necessary for successful remote memory recall.

To explore the role of the ADn, and its connections, at recent and remote time-points, here we used contextual fear conditioning. We found that the ADn is necessary for the retrieval of recent, but not remote, contextual fear memory. Consistent with this, retrieval-induced activity of ADn decreases as a function of memory age. We then identified a long-range inhibitory pathway from the CA3 subfield of the hippocampus to the ADn. This CA3–ADn inhibitory pathway is recruited during memory consolidation, and becomes necessary for the retrieval of remote fear memory. Previous studies have shown that consolidation of event memories involves gradual recruitment of brain regions over time. Our current results suggest that active disengagement of at least the ADn is additionally necessary for successful memory retrieval at remote time-points.

Results

ADn activity is necessary for recall of recently acquired memory.

We first assessed retrieval-induced activation of ADn as a function of memory age. To do this, we trained wild-type (WT) mice in contextual fear conditioning, and tested their memory at either 1 or 28 d post-training (Fig. 1a). At 90 min following testing, mice were perfused and we analyzed the expression of the activity-regulated gene, *Fos*, in the ADn. c-Fos expression was additionally assessed in three control groups of mice: (1) home-cage mice; (2) mice trained without a footshock and tested 1 or 28 d later; and (3) mice trained with an immediate shock and tested 1 or 28 d later. For all mice that were tested 1 or 28 d later, c-Fos levels were normalized to those levels in home-cage controls (Fig. 1b,c). In comparison with control mice, memory retrieval at 1 d post-training significantly increased the expression of c-Fos in the ADn. In contrast, c-Fos levels were not increased in mice tested at the 28-d time-point, and were equivalent to those in control mice. Consistent with a previous observation in rats[19], these results suggest that the ADn is actively engaged during retrieval of a recently, but not remotely, acquired fear memory. At remote time-points, the ADn may be either not engaged or, alternatively, actively disengaged or inhibited.

To test whether the activity of ADn is necessary for retrieval of a recent memory, we next inhibited the ADn cells optogenetically during retrieval of a contextual fear memory. As ADn contains excitatory neurons[24,25] (Extended Data Fig. 2), we micro-infused an adeno-associated virus (AAV) expressing the inhibitory opsin iC++ with a fluorescent reporter, EYFP, under the CaMKII promoter (AAV-CaMKII-iC++-EYFP) bilaterally in the ADn in WT mice (Fig. 1d). The iC++ opsin is a light-activated chloride channel that has improved chloride selectivity and conductivity compared with previous generations of inhibitory opsins using chloride pumps[26], and therefore allows efficient inhibition of targeted cells. Control mice received micro-infusion of a virus expressing only the fluorescent reporter (AAV-GFP). At 4 weeks following surgery, after allowing sufficient time for the virus to be expressed, mice were implanted with an optical fiber in the ADn, and trained in contextual fear conditioning. Contextual fear memory was tested either 1 or 28 d post-training. During the test, photo-stimulation was delivered during the last 3 min of a 6-min test session (Fig. 1e,f), allowing a within-animal comparison of the effect of inhibiting ADn cells during memory recall.

Inhibition of ADn cells during the 1-d test impaired memory retrieval. Mice infused with the iC++ virus froze less during the light-ON period than the light-OFF period, and also less than the control mice micro-infused with the GFP virus (Fig. 1e). In contrast, inhibition of ADn cells during the 28-d test had no effect on memory recall (Fig. 1f). In this case, mice infused with the iC++ virus froze at similar levels during the light-ON and light-OFF periods, and at equivalent levels to mice micro-infused with the control virus.

These results show that ADn is actively engaged and necessary for recent, but not remote, memory retrieval. These results extend previous experiments in which pharmacological inhibition of the anterior thalamus (including ADn) in rats impaired recall of recent, but not remote, contextual fear memory[19].

ADn receives inhibitory projections from CA3.

ADn may play no role in the remote recall of contextual fear conditioning. Alternatively, successful remote memory recall may involve active inhibition of ADn by one or more brain regions, and such inhibition may be necessary for successful remote memory retrieval. To explore this latter possibility, we next examined afferent input to the ADn. Retrobeads were unilaterally infused into the ADn, and retrogradely labeled neurons were identified (Fig. 2a). Consistent with previous findings[15,16,27–29], we found labeled neurons in layer VI of anterior cingulate cortex, retrosplenial cortex, and presubiculum, indicating that these regions send projections to the ADn (Extended Data Fig. 3a,b). In addition, we found retrogradely labeled neurons in the ipsilateral stratum pyramidale of CA3 subfield of the hippocampus (Fig. 2a,b).

To our knowledge, this CA3 to ADn projection has not been previously described. We therefore next sought to verify this connection using complementary tracing methods. We first micro-infused the retrograde tracer cholera toxin subunit B (CTB; Fig. 2c,d and Extended Data Fig. 3c,d) unilaterally in the ADn. Consistent with our Retrobeads analysis, retrogradely labeled neurons were found in the same regions, and specifically in the ipsilateral CA3 region of the hippocampus (Fig. 2d and Extended Data Fig. 3d). We next micro-infused the anterograde tracer phytohemagglutinin-L (PHA-L) unilaterally into the CA3 in a separate cohort of mice. We identified anterogradely labeled axons in the ipsilateral ADn, and also in ipsilateral CA1, and contralateral CA3 and CA1 (Fig. 2e,f and Extended Data Fig. 3e,f), as observed previously[30,31].

Because the ADn might be actively inhibited during remote memory recall, we next used three complementary approaches to assess whether CA3 sends inhibitory projections to the ADn. First, we micro-infused the retrograde tracer CTB unilaterally into the ADn, and performed immunohistochemical staining of CA3 sections using the inhibitory cell marker GAD67 (Fig. 3a,b). We found sparse labeling of CTB^+ cells in ipsilateral CA3 (2.5 ± 0.7 CTB^+ neurons per 10^5 mm^2 in CA3), with the majority of the CTB-labeled CA3 cells colocalized with GAD67.

Second, we used a viral tracing approach to label only the CA3–ADn projections and performed immunohistochemistry to investigate whether the projections are inhibitory. Specifically, we micro-infused AAVrg-Cre-EGFP unilaterally into ADn and AAV-DIO-mCherry bilaterally into CA3 (Fig. 2g,h). Using this approach, Cre is retrogradely transported from axon terminals in ADn to neuronal cell bodies, where Cre allows recombination and expression of mCherry exclusively in the CA3–ADn pathway. Consistent with our other tracing methods, we observed mCherry-labeled somas and axons in CA3 and ADn, respectively, specifically labeling the CA3–ADn projection neurons. The majority of the mCherry-labeled cells were observed in CA3 ipsilateral to the ADn infusion site 1.5–2.5 mm posterior to bregma, consistent with our other methods (Extended Data Fig. 3g,h). We further costained CA3 and ADn sections with GAD67 and VGAT, respectively, and found that many retrogradely labeled ($mCherry^+$) neurons in CA3 are inhibitory ($GAD67^+$), and many ($mCherry^+$) axons in ADn are inhibitory ($VGAT^+$) (Fig. 3e–g).

Third, we used an anterograde approach to examine inhibitory projections to the ADn. Specifically, we micro-infused an AAV that expresses the fluorescent reporter (EYFP) in a Cre-recombinase-dependent manner (AAV-DIO-EYFP) in mice expressing Cre-recombinase only in inhibitory (that is, $VGAT^+$) neurons (VGAT-Cre mice). We targeted cortical and hippocampal regions sending projections to the ADn, as identified by the analyses above (Fig. 2a–f and Extended Data Fig. 3a–d). These regions included CA3, retrosplenial cortex, presubiculum, and anterior cingulate cortex (Fig. 3c,d and Extended Data Fig. 3i–n). Dense terminal projection labeling in ADn was only observed following viral micro-infusions into CA3 (Fig. 3c,d). Together, these converging lines of evidence indicate that CA3 sends long-range, inhibitory projections to the ADn.

CA3 inhibitory cells projecting to the ADn become more active as memory ages.

One possibility is that this CA3–ADn inhibitory projection is active during remote memory recall, and the resulting suppression of ADn activity is necessary for successful memory retrieval. To test this hypothesis, we analyzed the expression of c-Fos in these CA3 inhibitory cells that project to the ADn during memory retrieval at 1 or 28 d post-training. We micro-infused a retrograde AAV (AAV-Ef1a-DO_DIO-TdTomato_EGFP-WPRE-pA) in the ADn of VGAT-Cre mice (Fig. 4a). This virus is retrogradely transported from the axon terminals to neuronal cell bodies, where the double-floxed orientation (DO) allows the expression of the fluorescent tag, TdTomato, only in the cells lacking Cre (Cre-Off). At the same time, the double-floxed inverted open reading frame (DIO) allows the expression of another fluorescent tag, EGFP, only in $VGAT^+$ cells (Cre-On)[32]. Therefore, using this approach, in CA3 we were able to simultaneously visualize both excitatory ($TdTomato^+$) and inhibitory ($EGFP^+$) ADn projection neurons.

Following micro-infusion in the ADn, mice were fear conditioned and then tested 1 or 28 d later (Fig. 4a). At 90 min after the test, mice were perfused, and we analyzed the expression of c-Fos in the excitatory ($TdTomato^+$) and inhibitory ($EGFP^+$) projection neurons in the CA3. We found that the retrieval-induced c-Fos expression was elevated in inhibitory CA3 neurons at the 28-d time-point in comparison with the 1-d time-point (Fig. 4b,c). There was no significant change in the activity of excitatory CA3 cells that project to the ADn across retrieval delays (Fig. 4d). Nor was there any change in the overall CA3 c-Fos expression following recent versus remote contextual fear memory recall (Fig. 4e), most likely reflecting the fact that neurons that project from CA3 to the ADn only represent a small fraction of all neurons in CA3. This result supports the hypothesis that the activity of CA3 inhibitory cells projecting to the ADn increases during remote memory recall.

The inhibitory pathway from CA3 to ADn is necessary for remote, but not recent, memory retrieval.

Since CA3 inhibitory neurons projecting to ADn become more active 28 d after training in comparison with 1 d, we hypothesized that CA3 may be inactivating the ADn during remote memory recall. To investigate this, we micro-infused the ADn with an AAV that expresses the fluorescent reporter (EYFP) with the inhibitory opsin iC++ in a Cre-recombinase-dependent manner (DIO) (AAV-DIO-iC++-EYFP) in VGAT-Cre mice. A different group of mice were micro-infused with a control virus that only contained the fluorescent tag

(AAV-DIO-EYFP). We then implanted an optical fiber above the ADn (Fig. 5a,b). We trained the mice in contextual fear conditioning and then tested their memory 1 or 28 d later. During the memory test, the laser was OFF during the first 3 min, then turned ON during the subsequent 3 min to inactivate the projection terminals of the CA3–ADn inhibitory cells.

At the 1-d delay, photo-stimulation did not alter freezing levels in either control or iC++ groups, suggesting that the CA3–ADn inhibitory pathway is not necessary for memory recall at this time-point (Fig. 5c). At the 28-d delay, however, while both control and iC++-infused mice froze equally during the OFF period, photo-stimulation reduced freezing in the iC++ group (Fig. 5d), suggesting that selective silencing of this inhibitory CA3–ADn projection impairs recall of remote contextual fear memory. We observed similar results in an independent replication of this experiment (Extended Data Fig. 4a–c). Inhibition of the CA3–ADn inhibitory pathway does not alter locomotor activity in either novel or familiar environments (tested either in the open field or in the conditioning context; Extended Data Fig. 5a–f). These data indicate that the photo-stimulation-induced reductions in freezing observed during the remote contextual memory test were not confounded by nonspecific locomotor effects.

We note that overall freezing levels were much lower in the 1-d test compared with the 28-d test. Reduced freezing at the recent delay was additionally observed in the independent replication of this experiment (Extended Data Fig. 4a–c). Because of reduced freezing levels in the 1-d test, it remains possible that potential effects of manipulating this inhibitory projection on recent memory are obscured by a floor effect. However, additional analyses suggest that freezing in the VGAT-Cre mice in the recent test reflects successful memory retrieval and that floor levels of freezing are much lower. First, freezing levels during the 1-d test were significantly higher than those during the preshock period during training (Extended Data Fig. 4e,f). Second, when a separate cohort of VGAT-Cre mice were trained without shocks they exhibited negligible freezing when tested 1 d later (Extended Data Fig. 4g), suggesting that ‘floor’ freezing is 0–1% in this strain. Third, behavioral (latent inhibition[33,34]; Extended Data Fig. 4h) and optogenetic (Fig. 5c,d and Extended Data Fig. 4b,c) interventions reduce freezing, even when control levels are 20–40%. Nonetheless, future experiments should verify that selective silencing of inhibitory CA3–ADn projections impairs remote memory in other mouse lines.

We also assessed how the activity of ADn changes when the CA3–ADn inhibitory projection was silenced following recent versus remote memory recall. Consistent with our previous analyses (Fig. 1b), retrieval-induced c-Fos expression was reduced at the remote, compared with recent, time-point in EYFP-infused mice. Importantly, retrieval-induced c-Fos expression was elevated in iC++-infused mice only at the remote time-point (Fig. 5e and Extended Data Fig. 4d). This result is consistent with our hypothesis that the CA3–ADn inhibitory projection becomes more active over time, such that it suppresses the activity of ADn during remote memory recall.

Together, our data show that the ADn becomes disengaged during memory consolidation. This disengagement is a result of recruitment of an inhibitory pathway from CA3 to ADn.

Importantly, activation of this CA3–ADn inhibitory pathway is necessary for successful remote fear memory recall.

Discussion

Event memories are supported by distributed hippocampal–thalamic–cortical networks[11], but the specific brain regions that contribute to memory expression may vary with memory age. While previous studies have examined the relationship between activation of brain regions and memory age at the time of recall[19,35–38], here we asked whether the active disengagement of one such brain region, the ADn, is necessary for recall, and, in addition, which projection(s) mediate such inhibition. Using a mouse contextual fear conditioning paradigm, we find that retrieval-induced activity of ADn is reduced at remote (28 d) compared with recent (1 d) time-points following training. We identified a sparse, long-range projection from inhibitory CA3 neurons to the ADn, and find that retrieval-induced activity of these ADn projecting inhibitory neurons is increased from recent to remote memory recall. More importantly, inhibiting the CA3–ADn inhibitory pathway impairs memory recall only at the remote time-point.

As far as we know, this is the first time that this inhibitory anatomical projection has been identified, likely due to its sparsity. Here, using seven different tracing methods (including single-step, transneuronal, enzymatic, and viral anterograde and retrograde tracers), we provide convergent evidence for an inhibitory CA3–ADn projection. Despite its sparsity, we additionally show that this inhibitory CA3–ADn projection plays a critical role in the retrieval of remote contextual fear memory. While most of the GABAergic cells in the brain target local neurons, some examples of long-range inhibitory connections have also been previously reported. For example, there are bidirectional long-range GABAergic projections between the hippocampus (CA1, CA3 and DG) and entorhinal cortex[39], as well as between the hippocampus (CA1 and CA3) and medial septum[40,41]. In addition, CA1 GABAergic cells also project to the subiculum and retrosplenial cortex[42]. Functionally, these long-range inhibitory connections can modulate memory function in a number of different ways, for example, by modulating theta oscillations in the hippocampus that are critical for spatial memory[39], and by facilitating interregional temporal coordination of activity[42,43]. The CA3–ADn GABAergic connection that we identified here adds to the functional complexity of these long-range inhibitory connections.

Our initial motivation to focus on the ADn was based on our previous study which examined c-Fos expression induced in 84 different brain regions by recall of recent and remote contextual fear in mice[11]. By examining how c-Fos expression covaried across regions, this analysis identified collections of brain regions that were coactivated during recent and remote memory recall. One striking feature of these analyses was that whereas activity in the ADn was positively correlated with activity in other brain regions following recent memory recall, this pattern switched for remote memory recall, where activity in the ADn was negatively correlated with activity in other brain regions. Moreover, at the remote time-point, the region with the strongest negative correlation with the ADn was CA3. It is interesting to note that at the recent time-point, the correlation between CA3 and ADn was positive ($r = 0.64$, $P = 0.085$) in this earlier analysis, although not statistically significant[11]. This

is consistent with our observation that the inhibitory CA3–ADn pathway is not active or required for recent memory retrieval.

Our discovery of an inhibitory pathway from CA3 to the ADn may account for the differential role of ADn in recent versus remote memory retrieval (Extended Data Fig. 1). The activity of this projection is dynamically modulated by fear retrieval, with the CA3–ADn GABAergic projection cells being most strongly activated by remote memory recall. This increase in retrieval-induced activity coincides with a decrease in retrieval-induced ADn activation with memory age. More importantly, we provide causal evidence that the inhibition of ADn activity via the CA3–ADn pathway is necessary for remote memory recall. Consistent with previous studies, we observed that CA3 is equivalently active at recent (day-old) and remote contextual fear memory recall (month-old)[44]. However, our results additionally suggest that there is time-dependent recruitment of inhibitory CA3 neurons, and, in particular, those that project to ADn (Extended Data Fig. 6). Although we did not observe a statistically significant change in the activation level of the excitatory CA3–ADn projections over time, our data do not exclude the possibility that the excitatory projections also play a role in memory consolidation and retrieval.

Analysis of activity-dependent gene expression indicates that recall of recent and remote contextual fear memory engages different networks, with remote memory in particular engaging broad hippocampal–thalamic–cortical networks[11]. The emerging importance of the CA3–ADn inhibitory pathway in recall of contextual fear memory may reflect the switch from the recent to the remote network state. One possible mechanism for this switch is via a decrease in feedforward inhibition from DG to CA3 over time as memory ages[45,46]. Specifically, feedforward inhibition from DG to CA3 is initially increased after fear learning, but is reduced at the remote time-point. Reduced inhibition of CA3 could lead to enhanced activity in specific subpopulations of CA3 neurons, including the inhibitory CA3–ADn projection neurons that we studied here. Such a contribution of CA3 to remote memory expression is inconsistent with the idea that the hippocampus plays a time-limited role in expression of these types of memories[47]. In fact, more recent optogenetic[48,49] and imaging[44] studies suggest that the hippocampus contributes to remote memory recall. These studies, together with our current data, are consistent with models of systems consolidation that emphasize a prolonged role for the hippocampus in memory retrieval, even at remote time-points[50].

Methods

Mice.

All procedures were approved by the Canadian Council for Animal Care and the Animal Care Committees at the Hospital for Sick Children and the University of Toronto. Experiments were conducted on 8–12-week-old male and female F1 hybrid (C57BL/6NTac × 129S6/SvEvTac) WT mice, or VGAT-Cre knock-in transgenic mice where Cre-recombinase was targeted to the *VGAT* locus, without disrupting endogenous VGAT expression. The VGAT-Cre mice were obtained from The Jackson Laboratory. Heterozygous VGAT-Cre mice were maintained on a C57BL/6NTac × 129S6/SvEvTac genetic background.

All mice were weaned at 21 d, and group housed with 2–5 mice per cage in a temperature-controlled room with 12-h light/dark cycle (light on during the day). All experiments were performed between 8:00 and 12:00. Mice were given ad libitum access to food and water. Mice were randomly assigned to experimental groups. The experimenters were aware of the experimental group assignment, as the same experimenters conducted the training and testing of all mice, but were blinded during behavioral assessment and cell counting experiments. Mice were excluded from analysis based on postexperimental histology: only mice with robust expression of the viral vectors or tracers (as specified in each experiment) specifically in the targeted region were included.

Micro-infusion of viral vectors and tracers.

Various adeno-associated viral vectors (AAVs) and tracers were used, as specified in each experiment. All viral vectors were infused bilaterally at 1.2 μl per side and 0.1 μl min^{-1}, unless otherwise specified. Tracers were infused unilaterally at 0.5-μl volume and 0.1 μl min^{-1} (Retrobeads), 0.1-μl volume and 0.01 μl min^{-1} (CTB), or 0.05-μl volume and 0.01 μl min^{-1} (PHA-L).

Specifically, in Fig. 1, AAV8-CaMKII-iC++-EYFP virus was obtained from Stanford Neuroscience Gene Vector and Virus Core and micro-infused bilaterally in the ADn (−0.8 mm anteroposterior (AP), ±0.2 mm mediolateral (ML), −3 mm dorsoventral (DV), from bregma, according to Paxinos and Franklin[51]) of WT mice to allow optogenetic silencing of the ADn. The control group received ADn infusion of AAV(DJ)-CMV-GFP, where GFP is expressed under the CMV promoter (made in-house). At 4 weeks following surgery, optical fibers were placed above the ADn (−0.8 mm AP, ±0 mm ML, −2.7 mm DV).

In Figs. 2 and 3 and Extended Data Fig. 3, the retrograde tracer Retrobeads (red) was obtained from Lumafluor and micro-infused unilaterally in the ADn of WT mice to retrogradely label regions that send monosynaptic projections to the ADn. To verify the results obtained using Retrobeads, in separate cohorts of mice, we micro-infused another retrograde tracer, CTB (Thermo Fisher Scientific), into the ADn (Fig. 2 and Extended Data Fig. 3). Mice were perfused 14 d following surgery to visualize projection neurons. To verify these results with an anterograde tracer, we micro-infused PHA-L (Vector Laboratories) into the CA3. Mice were perfused 3 weeks following surgery to visualize projection neurons. We additionally verified the CA3–ADn projection by specifically labeling the projection using a dual-viral tracing approach. We micro-infused 0.5 μl of pENN-AAVrg-hSyn-H-eGFP-Cre-WPRE-SV40 (no. 105540-AAVrg, Addgene) unilaterally into ADn and 0.6 μl of AAV(DJ)-hSyn-DIO-mCherry bilaterally into CA3. Mice were perfused 4 weeks following surgery to visualize the CA3–ADn projection ($mCherry^{+}$) neurons.

In Fig. 4, AAVrg-EF1a-DO_DIO-TdTomato-EGFP was obtained from Addgene and micro-infused unilaterally in the ADn of VGAT-Cre mice to retrogradely label excitatory and inhibitory cells that project to the ADn. This construct allows Cre-dependent expression of EGFP, and expression of TdTomato in the absence of Cre[32]. The AAV is produced in a retrograde serotype to allow retrograde labeling of projection neurons to the site of injection.

In Fig. 5 and Extended Data Figs. 4 and 5, AAV(DJ)-EF1a-DIO-iC++-EYFP was obtained from Stanford Neuroscience Gene Vector and Virus Core and micro-infused bilaterally in CA3 (−2.2 mm AP, ±2.7 mm ML, −2.4 mm DV, from bregma, according to Paxinos and Franklin[51]) of VGAT-Cre mice. In this inhibitory opsin viral vector, the double-floxed inverted open reading frame of iC++ fused to EYFP can be expressed from the EF1a promoter after Cre-mediated recombination. At 4 weeks following surgery, optical fibers were placed above ADn to allow optogenetic silencing of CA3–ADn projections. The control group received infusion of AAV8-hSyn-DIO-EGFP (Addgene) in CA3 of VGAT-Cre mice, where the double-floxed inverted open reading frame of the EGFP fluorescence tag can be expressed from the human synapsin (hSyn) promoter after Cre-mediated recombination.

The micro-infusion surgery protocol is similar to that previously described[52]. Specifically, mice were pretreated with atropine sulfate (0.1 mg kg^{-1}, intraperitoneal), then anesthetized with chloral hydrate (400 mg kg^{-1}, intraperitoneal). Mice were then placed on a stereotaxic frame, and holes were drilled in the skull at the targeted coordinates. Viral vector was micro-infused at 0.1 μl min^{-1} via glass pipettes connected to a Hamilton microsyringe with polyethylene tubing. After micro-infusion, the glass pipette was left in the brain for another 5 min to allow sufficient time for the virus to diffuse. We have found that this infusion procedure produces high infection in the targeted region, without sizable spread outside the region of interest[52,53]. For infusions of CTB and PHA-L tracers, we followed a similar procedure but performed injections using a Nanoject III injector (Drummond Scientific) and left the pipette in the brain for 10–15 min following infusions to minimize spread of tracers outside of regions of interest. Mice were then treated with analgesic (ketoprofen, 5 mg kg^{-1}, subcutaneous) and 1 ml of 0.9% saline (subcutaneous).

For the optogenetic experiments, mice received optical fiber implant 4 weeks following viral infusion. Optical fibers were constructed in-house by attaching a 5-mm piece of 200-μm optical fiber (with a 0.37 numerical aperture) to a 1.25-mm zirconia ferrule (final fiber extended 3 mm beyond ferrule). Fibers were attached with epoxy resin into ferrules, cut and polished. Optical fibers were stabilized to the skull with screws and black dental cement to minimize light leakage. For the 1-d groups, viral infusion was performed 5 weeks before training/testing. For the 28-d groups, viral infusion was performed 1 week before contextual fear training, and 4 weeks before testing. Thus, for both 1-d and 28-d groups, the interval between viral infusion and testing was 5 weeks.

Behavioral experiments.

Behavioral experiments for mice that did not undergo viral micro-infusion were carried out in 8-week-old WT mice (Fig. 1a,b). Experiments for mice that were micro-infused with viral vectors started 1 week following optical fiber implant (5 weeks after micro-infusion).

Contextual fear conditioning.—WT mice were trained in a standard contextual fear conditioning paradigm, as previously described[54]. Mice were first habituated to the conditioning chamber for 120 s, then given three shocks (0.5 mA each, 60 s apart), and remained in the chamber for another 60 s following the last shock. The amount of time

mice spent freezing (percentage freezing, with minimum bout of 1 s) was monitored with overhead cameras, and calculated using automatic scoring software FreezeFrame v.3.32 (Actimetrics).

VGAT-Cre mice, when trained using the standard contextual fear conditioning protocol, froze less than the WT mice. Therefore, for the majority of experiments, VGAT-Cre mice were trained in an altered version of the contextual fear conditioning paradigm to ensure that they showed successful fear memory retrieval (significantly higher freezing levels in comparison with preshock; Extended Data Fig. 4e,f). Specifically, VGAT-Cre mice were habituated to the conditioning chamber for 5 min 1 d before training. On the day of training, mice were habituated to the chamber for 120 s, then given four shocks (0.7 mA each, pseudo-random intervals), and remained in the context for another 30 s following the last shock (Extended Data Fig. 4a–d). For the independent replication, we extended the habituation period to 2 d (10 min, twice per day), as preliminary data showed that this extended habituation protocol slightly reduced variability in freezing levels. All other training and testing protocols were otherwise identical.

At either 1 or 28 d following training, mice were placed back into the training context for 5 min, without shock. The amount of time mice spent freezing (percentage freezing) was monitored with overhead cameras, and manually scored by experimenters blinded to the group assignment of mice. For the optogenetic experiments, the test session was 6 min in duration, where the laser was OFF during the first 3 min, then turned ON during the last 3 min when continuous direct current blue laser photo-stimulation (473 nm, 10-mW power) was applied.

c-Fos analysis.—To examine how the activity of ADn changes from recent (1 d) to remote (28 d) memory retrieval (Fig. 1a,b), we trained WT mice in contextual fear conditioning and tested them either 1 or 28 d later. At 90 min post-test, mice were perfused, and their brains used for c-Fos staining (see below). We analyzed c-Fos expression in the ADn in home-cage control mice, immediate-shock controls (one shock at 0.6 mA upon exposure to fear conditioning chamber, tested at 1 or 28 d post-training), no-shock controls (5 min exploration in fear conditioning chamber, tested at 1 or 28 d post-training) and those that underwent contextual fear conditioning (tested at 1 or 28 d post-training). For quantification and visualizations, c-Fos levels in all groups were normalized to averaged c-Fos in home-cage control mice.

To examine how the activity of the excitatory and inhibitory projection neurons from CA3 to ADn changes from recent to remote memory retrieval, VGAT-Cre mice were infused with the retrograde tracer AAVrg-EF1a-DO_DIO-TdTomato-EGFP. At 5 weeks following infusion, mice were trained in the contextual fear conditioning paradigm, and tested 1 d later. For the 28-d group, mice were trained in contextual fear conditioning 1 week following viral infusion, and tested 4 weeks later. At 90 min post-test, all mice were perfused, and their brains used for c-Fos staining. We analyzed c-Fos expression in the CA3–ADn projection neurons (excitatory and inhibitory), as well as total c-Fos in CA3, in home-cage control mice and those that underwent recent or remote memory test (Fig. 4).

Open field.—To control for the possibility that optogenetic manipulation of the CA3–ADn pathway alters locomotion in a novel environment, VGAT-Cre mice were micro-infused with AAV-DIO-iC++-EYFP or control virus (AAV-DIO-EYFP) in the CA3, then implanted with optical fibers in the ADn 4 weeks later. At 1 week after optical fiber implant, mice were placed in the center of an open square arena (45 × 45 × 20 cm^3 (length × width × height)) and allowed to explore for 6 min (ref. [55]), when the laser was OFF during the first 3 min, then turned ON during the last 3 min (Extended Data Fig. 5a,b). To control for the possibility that optogenetic manipulation of the CA3–ADn pathway alters locomotion in a familiar environment, VGAT-Cre mice were micro-infused with AAV-DIO-iC++-EYFP or control virus (AAV-DIO-EYFP) in the CA3, then implanted with optical fibers in the ADn 4 weeks later. At 1 week after optical fiber implant, mice were placed in the center of an open square arena (45 × 45 × 20 cm^3 (length × width × height)) and allowed to explore for 6 min (open field pre-exposure)[55] on day 1. After 24 h, mice were placed back into the same open field arena and allowed to explore for 6 min (open field test), when the laser was OFF during the first 3 min, then turned ON during the last 3 min (Extended Data Fig. 5c–e). We additionally assessed the effect of optogenetic inhibition of the CA3–ADn pathway on locomotion in a second familiar environment, the fear conditioning chamber (without shocks). VGAT-Cre mice were habituated to the fear conditioning chamber for 6 min without shocks, 1 d after open field test (fear chamber pre-exposure). At 24 h, mice were placed back into the same conditioning chamber to explore for 6 min (fear test), when the laser was OFF during the first 3 min, then turned ON during the last 3 min (Extended Data Fig. 5c,f). The location of the mouse was tracked using an overhead camera. The total distance traveled was assessed using ImageJ v.2.1.0 and freezing levels were assessed using FreezeFrame v.3.32 (Actimetrics).

Immunohistochemistry.

Immunofluorescence staining was conducted as previously described[56]. Specifically, at the end of behavior experiments, mice were transcardially perfused with 1× PBS followed by 4% paraformaldehyde. For the c-Fos experiment, mice were perfused 90 min after behavior test or training. Brains were fixed overnight at 4 °C, and transferred to 30% sucrose solution for 48 h. Brains were sectioned coronally using a cryostat (Leica CM1850), and 50-Mm sections were obtained for the ADn or hippocampus.

For αCaMKII and GAD67 immunostaining, free-floating sections were blocked with PBS containing 2.5% bovine serum albumin and 0.3% Triton-X for 30 min. Afterwards, sections were incubated in PBS containing mouse anti-αCaMKII primary antibody (1:200 dilution; Sigma Cat. no. C265 RRID:AB_258808) or mouse anti-GAD67 (1:500 dilution; EMD Millipore Cat. no. MAB5406 RRID: AB_2278725) primary antibody for 24 h at 4 °C. Sections were washed with PBS (three times), then incubated with PBS containing goat anti-mouse ALEXA Fluor 488 (1:500 dilution; Thermo Fisher Scientific Cat. no. A-11001 RRID:AB_2534069) secondary antibody for 24 h at 4 °C. Sections were washed with PBS, mounted on gel-coated slides and coverslipped with Vectashield fluorescent mounting medium (Vector Laboratories). Images were obtained using a confocal laser scanning microscope (LSM 710; Zeiss) with a ×20 objective.

For c-Fos immunostaining, free-floating sections were blocked with PBS containing 2.5% bovine serum albumin and 0.3% Triton-X for 30 min. Afterwards, sections were incubated in PBS containing rabbit polyclonal anti-c-Fos primary antibody (1:1,000 dilution; Santa Cruz Biotechnology Cat. no. sc-52 RRID:AB_2106783) for 48 h at 4 °C. Sections were washed with PBS (three times), then incubated with PBS containing goat anti-rabbit ALEXA Fluor 633 (for c-Fos, 1:500 dilution; Thermo Fisher Scientific Cat. no. A-21070 RRID:AB_2535731) secondary antibody for 24 h at 4 °C. Sections were washed with PBS, mounted on gel-coated slides and coverslipped with Vectashield fluorescent mounting medium (Vector Laboratories). Images were obtained using a confocal laser scanning microscope (LSM 710; Zeiss) with a ×20 objective.

For cell counting experiments in ADn and CA3, every section in ADn or every second section in CA3 was assessed for c-Fos$^+$ cells. Approximately 4–6 sections per mouse were counted and averaged, with 6–10 mice per group. To evaluate the activity in ADn or CA3 following recent versus remote memory test, the number of c-Fos$^+$ cells in ADn or CA3 (total number of c-Fos$^+$ cells per 10,000 μm^2) was counted. To evaluate the activity of CA3 to ADn projection neurons, c-Fos colocalization in TdTomato$^+$ cells (excitatory connections; total numbers of c-Fos$^+$ and TdTomato$^+$ cells per μm^3) or c-Fos colocalization in EGFP$^+$ cells (inhibitory connections; total numbers of c-Fos$^+$ and EGFP$^+$ cells per μm^3) was calculated. All results were then normalized to values obtained in home-cage control groups (3–8 animals) in respective cell populations.

To visualize CTB retrogradely labeled cells, brain sections were blocked as described above and then incubated with rabbit anti-CTB (1:1,000 dilution; Abcam Cat. no. ab34992 RRID: AB_726859) and mouse anti-GAD67 (1:500 dilution; EMD Millipore Cat. no. MAB5406 RRID: AB_2278725) primary antibodies for 48 h at 4 °C. Sections were washed with PBS (three times), then incubated with PBS containing goat anti-rabbit ALEXA Fluor 633 (for CTB, 1:500 dilution; Thermo Fisher Scientific Cat. no. A-21070 RRID:AB_2535731) and goat anti-mouse ALEXA Fluor 488 (for GAD67, 1:500 dilution; Thermo Fisher Scientific Cat. no. A-11001 RRID:AB_2534069) secondary antibodies for 24 h at 4 °C. Sections were washed with PBS, mounted on gel-coated slides and coverslipped with Vectashield fluorescent mounting medium (Vector Laboratories). Images were obtained using a confocal laser scanning microscope (LSM 710; Zeiss) with ×20 and ×40 objectives. To visualize PHA-L anterogradely labeled cells, brain sections were costained with PHA-L antibody. Specifically, brain sections were blocked as described above and incubated with rabbit anti-PHA (E + L) primary antibody (1:1,000 dilution; Vector Laboratories Cat. no. AS-2300–1 RRID: AB_2313686) for 24 h at 4 °C. Sections were washed with PBS (three times), then incubated with PBS containing goat anti-rabbit ALEXA Fluor 488 (1:500 dilution; Thermo Fisher Scientific Cat. no. A-11008 RRID:AB_143165) secondary antibody for 24 h at 4 °C. Sections were washed with PBS, mounted on gel-coated slides and coverslipped with Vectashield fluorescent mounting medium (Vector Laboratories). Images were obtained using a confocal laser scanning microscope (LSM 710; Zeiss) with ×20 and ×40 objectives.

To specifically visualize CA3–ADn projection neurons, brain sections containing CA3 from mice infused with AAVrg-Cre-EGFP and AAV(DJ)-hSyn-DIO-mCherry (unilaterally in ADn and bilaterally in CA3, respectively) were blocked as described above and then

incubated with rabbit anti-RFP (for mCherry, 1:1,000 dilution; Rockland Cat. no. 600–401-379 RRID: AB_2209751) and mouse anti-GAD67 (1:500 dilution; EMD Millipore Cat. no. MAB5406 RRID: AB_2278725) for 48 h at 4 °C. Sections were washed with PBS (three times), then incubated with PBS containing goat anti-rabbit ALEXA Fluor 568 (for mCherry, 1:500 dilution; Thermo Fisher Scientific Cat. no. A-11011 RRID:AB_143157) and goat anti-mouse ALEXA Fluor 647 (for GAD67, 1:500 dilution; Thermo Fisher Scientific Cat. no. A-21235 RRID: AB_2535804) secondary antibodies for 24 h at 4 °C. To visualize the projection terminals of the same neurons, sections containing the ADn from the same brains were blocked and then incubated with mouse anti-RFP (1:1,000 dilution; Rockland Cat. no. 200–301-379 RRID: AB_2611063) and rabbit anti-VGAT (1:500 dilution; EMD Millipore Cat. no. AB2257 RRID: AB_1587623) primary antibodies for 48 h at 4 °C. Sections were washed with PBS (three times), then incubated with PBS containing goat anti-mouse ALEXA Fluor 568 (for mCherry, 1:500 dilution; Thermo Fisher Scientific Cat. no. A-11004 RRID:AB_2534072) and goat anti-rabbit ALEXA Fluor 633 (for VGAT, 1:500 dilution; Thermo Fisher Scientific Cat. no. A-21070 RRID:AB_2535731) secondary antibodies for 24 h at 4 °C. Sections were washed with PBS, mounted on gel-coated slides and coverslipped with Vectashield fluorescent mounting medium (Vector Laboratories). Images were obtained using a confocal laser scanning microscope (LSM 710; Zeiss) with ×20, ×40 and ×100 objectives.

Statistics.

No statistical tests were used to predetermine sample size, but our sample sizes are similar to those reported in previous publications[49,53,57]. Data were analyzed using parametric two-way repeated measures analysis of variance (ANOVA), or two-sample Student's unpaired *t*-test. For comparisons with a hypothetical mean of 1, one-sample *t*-test was used. Where appropriate, ANOVA was followed by post hoc pairwise comparisons with Bonferroni correction. If data were significantly non-normal (with $\alpha = 0.05$) or variances were unequal, Kruskal–Wallis test or Mann–Whitney test (between-group comparisons) and Wilcoxon signed-rank test (within-group comparisons) were used accordingly. All tests were two-sided. Statistical analyses were performed using GraphPad Prism v.8.

Reporting Summary.

Further information on research design is available in the Nature Research Reporting Summary linked to this article.

Data availability

The data generated during and/or analyzed during the current study are available from the corresponding author on reasonable request.

Extended Data

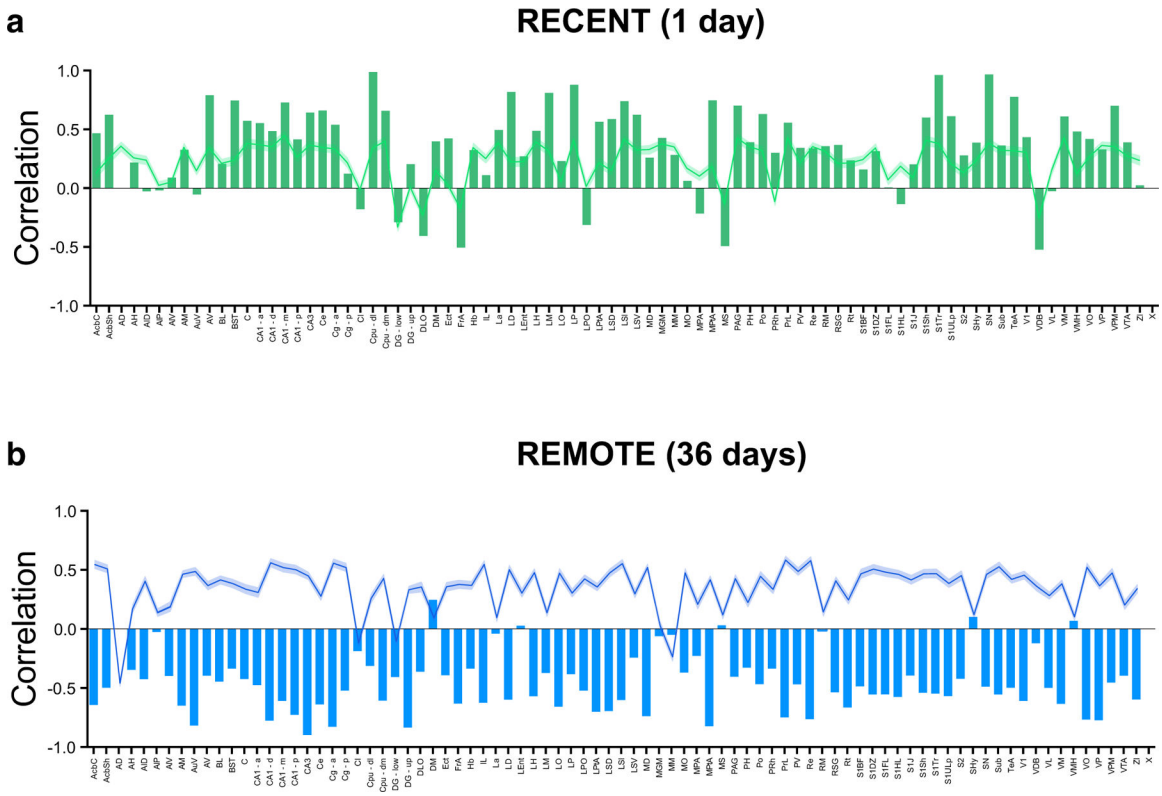

Extended Data Fig. 1 |. Analysis of co-activation of ADn with 83 other brain regions following recent vs. remote fear memory retrieval.

a, Following recent fear memory recall, ADn activity was positively correlated with activity in the majority of the other 83 brain regions. (bars: correlation between ADn and a given region; green line and shaded region: mean correlation between other 83 non-ADn brain regions and a given region ± s.e.m,). **b**, At the remote time point, ADn activity became strongly inversely correlated with activity in the majority (78/83) of other 83 brain regions. (bars: correlation between ADn and a given region; blue line and shaded region: mean correlation between other 83 brain regions combined and a given region ± s.e.m.). Data were obtained from Wheeler et al., 2013[11].

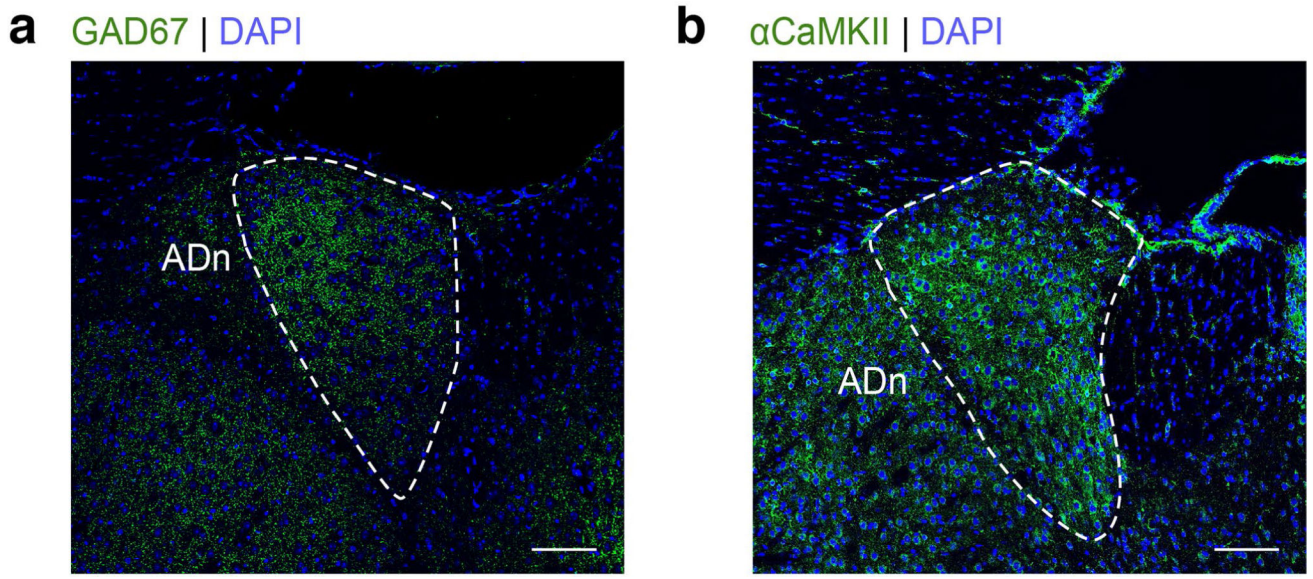

Extended Data Fig. 2 |. characterization of ADn cell type.
Representative images showing immunohistochemical staining in ADn of WT home cage mice with **a**, inhibitory cell marker GAD67 (repeated in $n = 3$), or **b**, excitatory cell marker aCamKII (repeated in $n = 3$; scale bar: 100 μm).

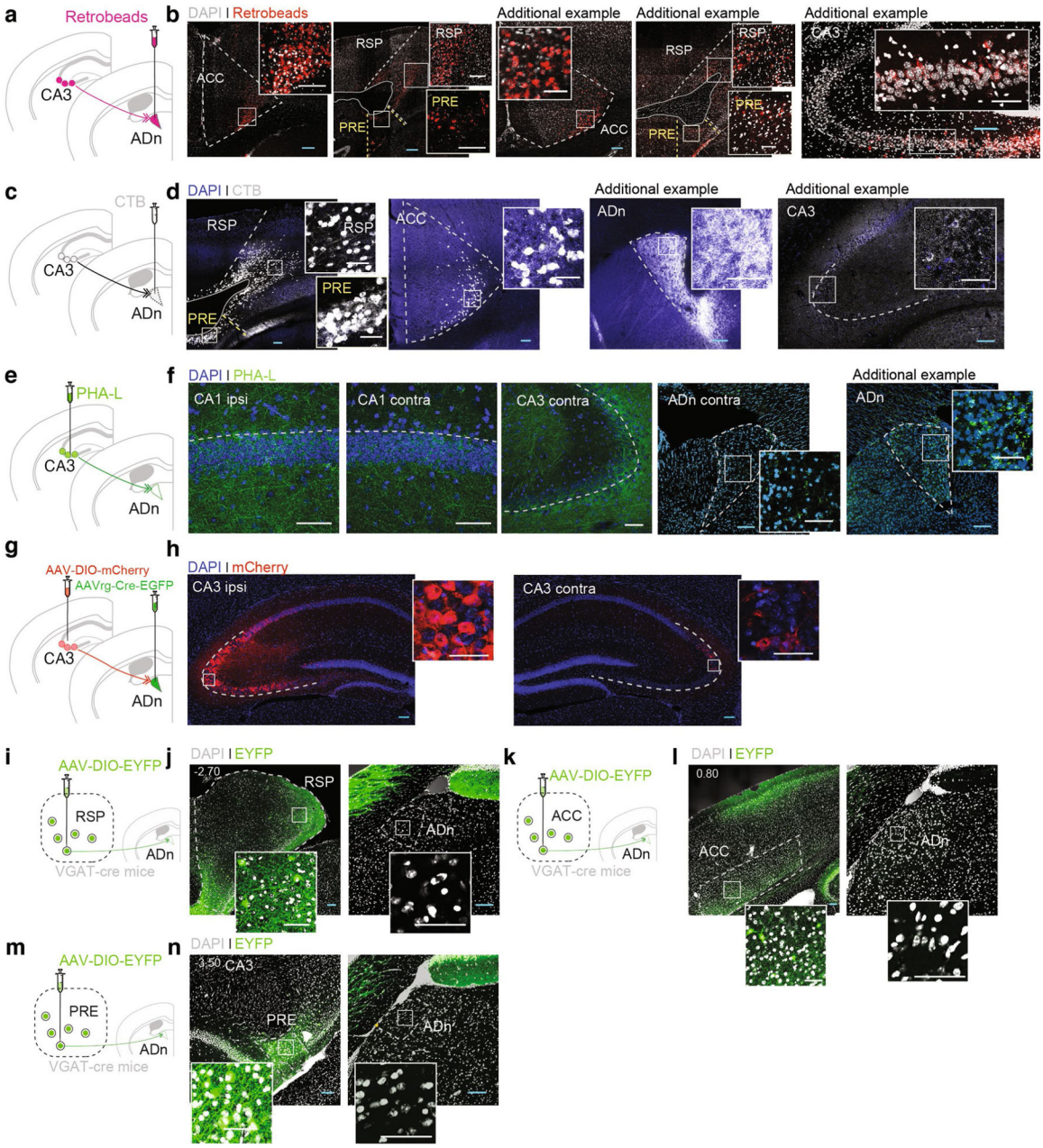

Extended Data Fig. 3 |. Identification of anatomical projections to the ADn.

a, WT mice were micro-infused with Retrobeads in the ADn, and **b**, neurons in anterior cingulate cortex (ACC), retrosplenial cortex (RSP), and presubiculum (PRE) were retrogradely labeled ($n = 3$). Examples from additional mice are included. **c**, WT mice were micro-infused with the retrograde tracer cholera toxin subunit B (CTB) in the ADn, and **d**, neurons in retrosplenial cortex (RSP), and presubiculum (PRE) were retrogradely labeled ($n = 3$). Additional examples of ADn infusion site and retrogradely labeled CA3 are also shown. **e**, WT mice were micro-infused with the anterograde tracer PHA-L in the CA3, and **f**, in addition to ipsilateral ADn (Fig. 2f), ipsilateral CA1, contralateral CA1 and CA3 were anterogradely labeled, while much less labeling was observed in contralateral ADn (*n*

= 4). An additional example of anterograde labeling in ADn is shown. **g-h**, To visualize specifically CA3-ADn projections, WT mice were micro-infused with AAV-DIO-mCherry bilaterally in CA3 and AAVrg-Cre-EGFP unilaterally in ADn (n = 4). Majority of the CA3-ADn (mCherry+) cells were visualized in CA3 ipsilateral to the site of ADn infusion. To see whether anatomical projections from other regions to ADn are inhibitory, different VGAT-Cre mice were micro-infused with AAV-DIO-EYFP in **i-j**, retrosplenial cortex (RSP), **k-l**, anterior cingulate cortex (ACC), or **m-n**, presubiculum (PRE) (n = 3 for each region). Unlike the CA3 (Fig. 3c,d), none of these regions showed terminal projections in the ADn (blue scale bars: 100 μm, white scale bars: 50 μm).

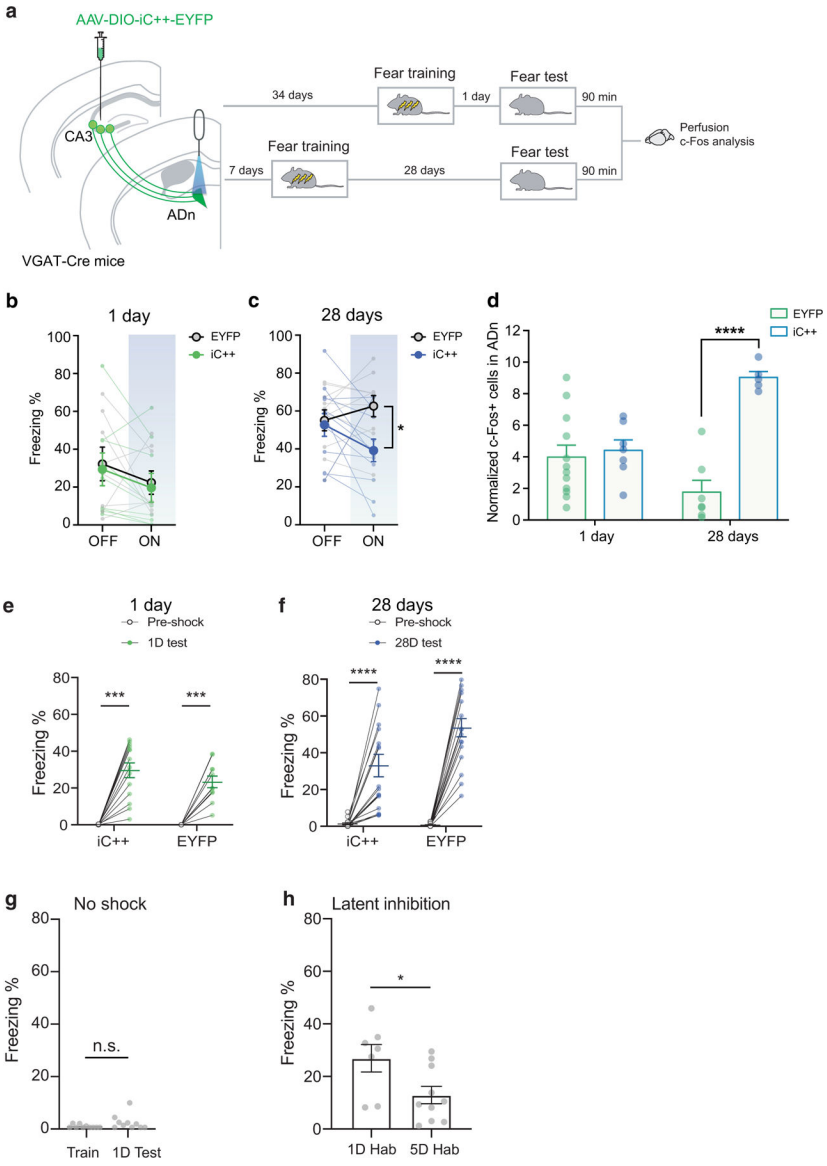

Extended Data Fig. 4 |. Independent replication experiment showing that cA3 inhibitory cells projecting to the ADn are necessary for the recall of remote memory.

a, VGAT-Cre mice were micro-infused with AAV-DIO-iC++-EYFP or AAV-DIO-EYFP virus in CA3 and optical fibres were implanted in the ADn, to optogenetically inhibit the

CA3-ADn projection during fear memory test, at 1 or 28 days post-training. **b**, At 1 day test, iC++- and EYFP-infused mice froze equally during light-OFF and light-ON epochs (iC++ $n = 9$; EYFP $n = 8$; two-sided Mann-Whitney test iC++ versus EYFP, $P = 0.40$; OFF: two-sided Wilcoxon signed rank test iC++ versus EYFP, $P = 0.82$; ON: two-sided Wilcoxon signed rank test iC++ versus EYFP, $P = 0.28$). **c**, At 28 day test, iC++- and EYFP-infused mice froze equally during light-OFF epoch (3 minutes duration), but iC++-infused mice showed reduced freezing in comparison to EYFP-infused mice during light-ON epoch (3 minute duration) (iC++ $n = 12$; EYFP $n = 10$; two-way repeated measures ANOVA iC++ versus EYFP x light-OFF versus light-ON; interaction, $F_{1,20} = 5.35$, $P = 0.031$; light-OFF versus light-ON, $F_{1,20} = 0.43$, $P = 0.52$; iC++ versus EYFP, $F_{1,20} = 3.45$, $P = 0.078$; *post hoc* Bonferroni's test, light-OFF iC++ versus EYFP $P > 0.99$, light-ON iC++ versus EYFP $P = 0.015$). **d**, At 1 day, iC++-infused mice showed equivalent level of c-Fos expression in the ADn (normalized to mean expression level in home cage control mice ($n = 16$)), in comparison to EYFP-infused control mice. But at 28 day, iC++-infused mice showed elevated level of c-Fos expression in the ADn, in comparison to controls. (1 day: iC++ $n = 7$; EYFP $n = 12$; 28 day: iC++ $n = 5$; EYFP $n = 7$; two-way ANOVA iC++ versus EYFP x 1 day versus 28 day; interaction, $F_{1,27} = 18.39$, $P = 0.0002$; 1 day versus 28 day, $F_{1,27} = 2.26$, $P = 0.14$; iC++ versus EYFP, $F_{1,27} = 23.34$, $P < 0.0001$; *post hoc* Bonferroni's test, 1 day iC++ versus EYFP $P > 0.99$, 28 day iC++ versus EYFP $P < 0.0001$). **e**, Both iC++ and EYFP groups froze significantly more during test (first 3 minutes) at 1 day than pre-shock period during training (iC++ $n = 14$; EYFP $n = 11$; iC++: two-sided Wilcoxon matched-pair signed rank test pre-shock versus 1 day test, $P = 0.0001$; EYFP: two-sided Wilcoxon matched-pair signed rank test pre-shock versus 1 day test, $P = 0.001$). **f**, Both iC++ and EYFP groups froze significantly higher during test (last 3 minutes) at 28 day than pre-shock period during training (iC++ $n = 18$; EYFP $n = 17$; iC++: two-sided Wilcoxon matched-pair signed rank test pre-shock versus 28 day test, $P < 0.0001$; EYFP: two-sided Wilcoxon matched-pair signed rank test pre-shock versus 28 day test, $P < 0.0001$). **g**. VGAT-Cre mice trained without shocks and tested the following day showed baseline (floor) level freezing ($n = 10$; two-sided paired *t*-tests $t_9 = 1.56$, $P = 0.15$). **h**. VGAT-Cre mice were habituated to the training context for 5 days (twice a day, 10 min each) before contextual fear conditioning. Mice showed significantly lower levels of freezing following this latent inhibition protocol, in comparison to the 1 day habituation protocol (1 day habituation (1D Hab): $n = 7$; 5 day habituation (5D Hab): $n = 10$; two-sided *t*-tests $t_{15} = 2.38$, $P = 0.03$). Data are individual mouse, or mean ± s.e.m. (* $P < 0.05$, *** $P < 0.001$, **** $P < 0.0001$).

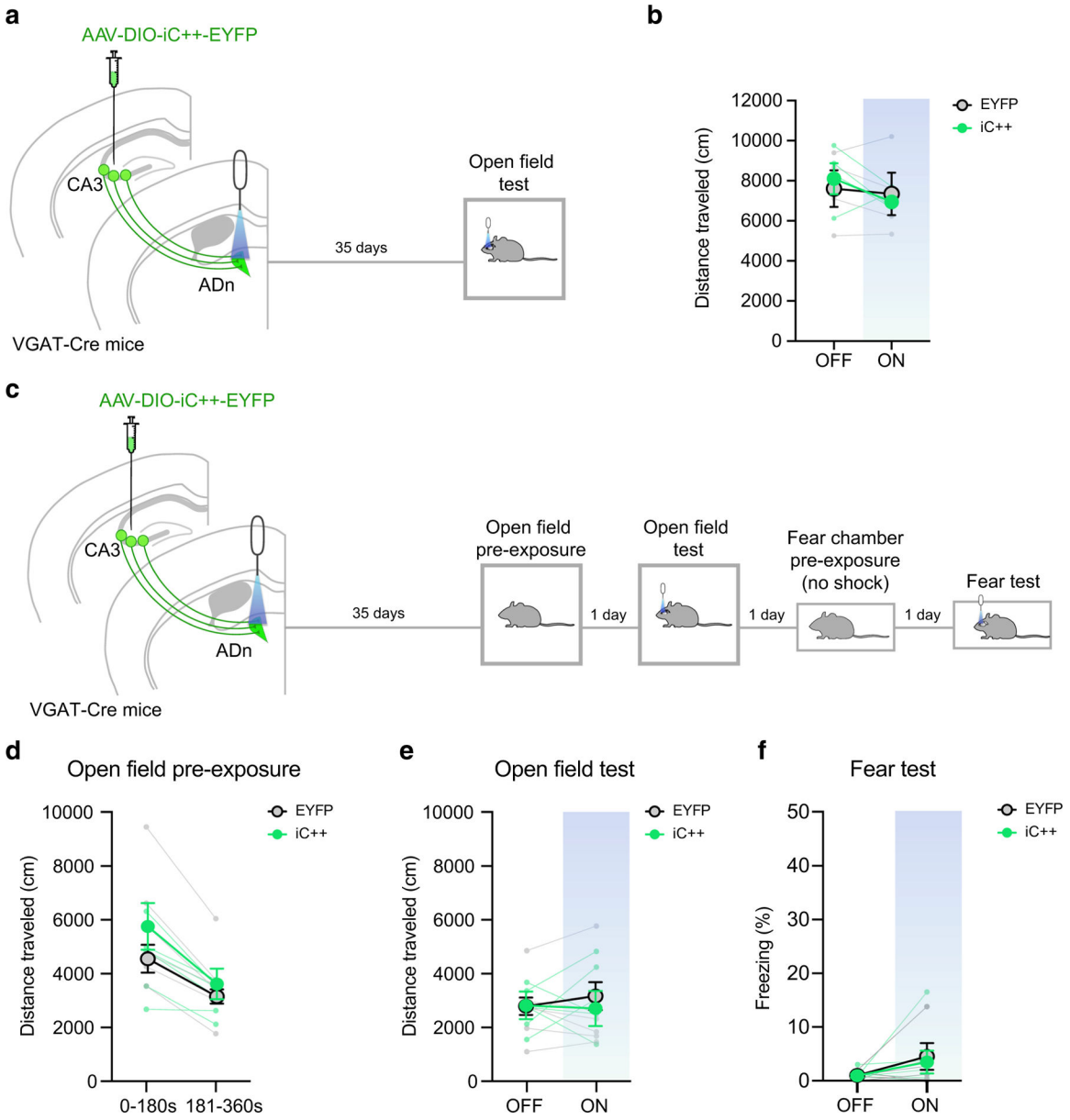

Extended Data Fig. 5 |. Inhibition of cA3-ADn inhibitory pathway does not alter locomotor activity in open field test.

a, VGAT-Cre mice were micro-infused with AAV-DIO-iC++-EYFP or AAV-DIO-EYFP virus in CA3 and optical fibres were implanted in the ADn, to optogenetically inhibit the CA3-ADn projection during test in a novel open field. **b**, iC++- and EYFP-infused mice showed similar levels of distance traveled during the light-OFF and light-ON epochs (3 minute duration) (iC++ $n = 4$; EYFP $n = 4$; two-way repeated measures ANOVA iC++ versus EYFP x light-OFF versus light-ON; interaction, $F_{1,6} = 0.92$, $P = 0.38$; light-OFF versus light-ON, $F_{1,6} = 2.31$, $P = 0.179$; iC++ versus EYFP, $F_{1,6} = 0.002$, $P = 0.97$). **c**, VGAT-Cre mice were micro-infused with AAV-DIO-iC++-EYFP or AAV-DIO-EYFP virus in CA3 and optical fibres were implanted in the ADn. On day 1, mice were pre-exposed to open field chamber without light (6 min), then on day 2, the CA3-ADn projection was

optogenetically inhibited by turning on the laser during the last 3 min of the open field test, to assess the effect of inhibition on locomotor activity in a familiar environment. To assess the effect of inhibition on locomotor activity in a second familiar environment, 1 day after open field test, mice were pre-exposed to the fear conditioning chamber without shocks and without light (6 min), and then 24 hours later, the CA3-ADn projection was optogenetically inhibited by turning on the laser during the last 3 min of the fear test. **d**, iC++- and EYFP-infused mice showed similar levels of distance traveled during the first and last 3 minutes of open field pre-exposure on day 1 without light (iC++ $n = 6$; EYFP $n = 6$; two-way repeated measures ANOVA iC++ versus EYFP x first-3-min versus last-3-min; interaction, $F_{1,10} = 2.05$, $P = 0.18$; first-3-min versus last-3-min, $F_{1,10} = 48.40$, $P < 0.0001$; iC++ versus EYFP, $F_{1,10} = 1.08$, $P = 0.32$). **e**, iC++- and EYFP-infused mice showed similar levels of distance traveled during light-OFF and light-ON periods of open field test on day 2 (iC++ $n = 6$; EYFP $n = 6$; two-way repeated measures ANOVA iC++ versus EYFP x light-OFF versus light-ON; interaction, $F_{1,10} = 0.54$, $P = 0.48$; light-OFF versus light-ON, $F_{1,10} = 0.15$, $P = 0.70$; iC++ versus EYFP, $F_{1,10} = 0.11$, $P = 0.74$). **f**, iC++- and EYFP-infused mice showed similar levels of freezing during light-OFF and light-ON periods of fear test 1 day after fear chamber pre-exposure without shocks (iC++ $n = 6$; EYFP $n = 6$; two-way repeated measures ANOVA iC++ versus EYFP x light-OFF versus light-ON; interaction, $F_{1,10} = 0.00$, $P = 0.77$; light-OFF versus light-ON, $F_{1,10} = 3.40$, $P = 0.09$; iC++ versus EYFP, $F_{1,10} = 0.00$, $P = 0.76$). Data are individual mouse, or mean ± s.e.m.

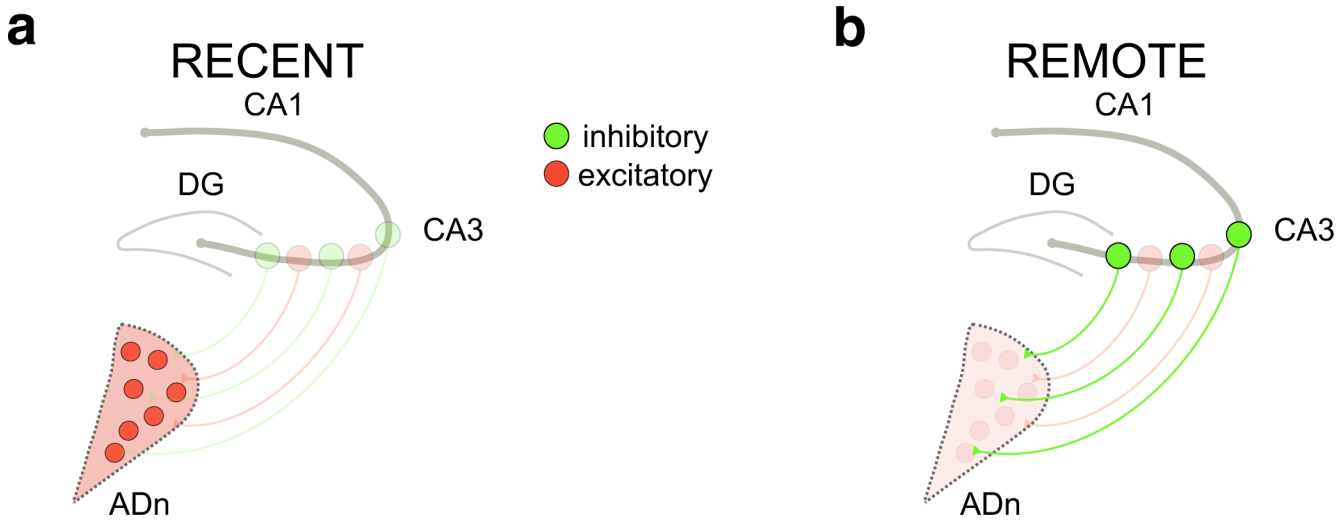

Extended Data Fig. 6 |. cA3-ADn pathway is recruited from recent to remote fear memory recall. **a**, ADn is activated and necessary for recent memory retrieval. At this time, the inhibitory cells that project from CA3 to the ADn are relatively inactive. **b**, At the remote memory retrieval, inhibitory cells that project from CA3 to the ADn are actively engaged to suppress the activity in ADn. The suppression of ADn activity is necessary for remote memory retrieval.

Acknowledgements

This work was supported by Canadian Institutes of Health Research (CIHR) grants to P.W.F. (grant no. FDN143227) and S.A.J. (grant no. MOP74650). F.X. was supported by fellowships from NSERC and Biological

Sleep and Rhythms (CIHR). G.V. was supported by the Biological Sleep and Rhythms (CIHR) fellowship. A.I.R. was supported by fellowships from NSERC and NIMH (grant no. 1 F31 MH120920-01). L.M.T. was supported by fellowships from The Hospital for Sick Children RestraComp and NSERC. P.W.F. and S.A.J. are senior fellows in the Child Brain & Development Program and the Brain, Mind & Consciousness programs, respectively, at the Canadian Institute for Advanced Research.

References

1. Buzsaki G The hippocampo-neocortical dialogue. Cereb. Cortex 6, 81–92 (1996). [PubMed: 8670641]
2. Frankland PW & Bontempi B The organization of recent and remote memories. Nat. Rev. Neurosci. 6, 119–130 (2005). [PubMed: 15685217]
3. Squire LR & Alvarez P Retrograde amnesia and memory consolidation: a neurobiological perspective. Curr. Opin. Neurobiol. 5, 169–177 (1995). [PubMed: 7620304]
4. Tonegawa S, Morrissey MD & Kitamura T The role of engram cells in the systems consolidation of memory. Nat. Rev. Neurosci. 19, 485–498 (2018). [PubMed: 29970909]
5. Jin J & Maren S Prefrontal-hippocampal interactions in memory and emotion. Front. Syst. Neurosci. 9, 170 (2015). [PubMed: 26696844]
6. Moscovitch M, Nadel L, Winocur G, Gilboa A & Rosenbaum RS The cognitive neuroscience of remote episodic, semantic and spatial memory. Curr. Opin. Neurobiol. 16, 179–190 (2006). [PubMed: 16564688]
7. Preston AR & Eichenbaum H Interplay of hippocampus and prefrontal cortex in memory. Curr. Biol. 23, R764–R773 (2013). [PubMed: 24028960]
8. Restivo L, Vetere G, Bontempi B & Ammassari-Teule M The formation of recent and remote memory is associated with time-dependent formation of dendritic spines in the hippocampus and anterior cingulate cortex. J. Neurosci. 29, 8206–8214 (2009). [PubMed: 19553460]
9. Simons JS & Spiers HJ Prefrontal and medial temporal lobe interactions in long-term memory. Nat. Rev. Neurosci. 4, 637–648 (2003). [PubMed: 12894239]
10. Tanaka KZ et al. Cortical representations are reinstated by the hippocampus during memory retrieval. Neuron 84, 347–354 (2014). [PubMed: 25308331]
11. Wheeler AL et al. Identification of a functional connectome for long-term fear memory in mice. PLoS Comput. Biol. 9, e1002853 (2013). [PubMed: 23300432]
12. Marshall L & Born J The contribution of sleep to hippocampus-dependent memory consolidation. Trends Cogn. Sci. 11, 442–450 (2007). [PubMed: 17905642]
13. Vetere G et al. Chemogenetic interrogation of a brain-wide fear memory network in mice. Neuron 94, 363–374.e4 (2017). [PubMed: 28426969]
14. Aggleton JP et al. Hippocampal-anterior thalamic pathways for memory: uncovering a network of direct and indirect actions. Eur. J. Neurosci. 31, 2292–2307 (2010). [PubMed: 20550571]
15. Child ND & Benarroch EE Anterior nucleus of the thalamus: functional organization and clinical implications. Neurology 81, 1869–1876 (2013). [PubMed: 24142476]
16. Jankowski MM et al. The anterior thalamus provides a subcortical circuit supporting memory and spatial navigation. Front. Syst. Neurosci. 7, 45 (2013). [PubMed: 24009563]
17. Aggleton JP, Hunt PR, Nagle S & Neave N The effects of selective lesions within the anterior thalamic nuclei on spatial memory in the rat. Behav. Brain Res. 81, 189–198 (1996). [PubMed: 8950016]
18. Harvey RE, Thompson SM, Sanchez LM, Yoder RM & Clark BJ Post-training inactivation of the anterior thalamic nuclei impairs spatial performance on the radial arm maze. Front. Neurosci. 11, 94 (2017). [PubMed: 28321178]
19. Lopez J, Gamache K, Milo C & Nader K Differential role of the anterior and intralaminar/lateral thalamic nuclei in systems consolidation and reconsolidation. Brain Struct. Funct. 223, 63–76 (2018). [PubMed: 28710525]
20. Mair RG, Burk JA & Porter MC Impairment of radial maze delayed nonmatching after lesions of anterior thalamus and parahippocampal cortex. Behav. Neurosci. 117, 596–605 (2003). [PubMed: 12802887]

21. Mitchell AS & Dalrymple-Alford JC Lateral and anterior thalamic lesions impair independent memory systems. Learn. Mem. 13, 388–396 (2006). [PubMed: 16741289]
22. van Groen T, Kadish I & Michael Wyss J Role of the anterodorsal and anteroventral nuclei of the thalamus in spatial memory in the rat. Behav. Brain Res. 132, 19–28 (2002). [PubMed: 11853854]
23. Viejo G & Peyrache A Precise coupling of the thalamic head-direction system to hippocampal ripples. Nat. Commun. 11, 2524 (2020). [PubMed: 32433538]
24. Nakamura Y et al. Immunohistochemical study of the distribution of Ca^{2+}/calmodulin-dependent protein kinase phosphatase in the rat central nervous system. Brain Res. Mol. Brain Res. 77, 76–94 (2000). [PubMed: 10814834]
25. Princivalle A, Regondi MC, Frassoni C, Bowery NG & Spreafico R Distribution of GABA(B) receptor protein in somatosensory cortex and thalamus of adult rats and during postnatal development. Brain Res. Bull. 52, 397–405 (2000). [PubMed: 10922519]
26. Berndt A et al. Structural foundations of optogenetics: determinants of channelrhodopsin ion selectivity. Proc. Natl Acad. Sci. USA 113, 822–829 (2016). [PubMed: 26699459]
27. Bienkowski MS et al. Integration of gene expression and brain-wide connectivity reveals the multiscale organization of mouse hippocampal networks. Nat. Neurosci. 21, 1628–1643 (2018). [PubMed: 30297807]
28. Shibata H & Naito J Organization of anterior cingulate and frontal cortical projections to the anterior and laterodorsal thalamic nuclei in the rat. Brain Res. 1059, 93–103 (2005). [PubMed: 16157311]
29. Vertes RP Analysis of projections from the medial prefrontal cortex to the thalamus in the rat, with emphasis on nucleus reuniens. J. Comp. Neurol. 442, 163–187 (2002). [PubMed: 11754169]
30. Finnerty GT & Jefferys JG Functional connectivity from CA3 to the ipsilateral and contralateral CA1 in the rat dorsal hippocampus. Neuroscience 56, 101–108 (1993). [PubMed: 8232909]
31. Witter MP Intrinsic and extrinsic wiring of CA3: indications for connectional heterogeneity. Learn. Mem. 14, 705–713 (2007). [PubMed: 18007015]
32. Saunders A, Johnson CA & Sabatini BL Novel recombinant adeno-associated viruses for Cre activated and inactivated transgene expression in neurons. Front. Neural Circuits 6, 47 (2012). [PubMed: 22866029]
33. Kiernan MJ & Westbrook RF Effects of exposure to a to-be-shocked environment upon the rat's freezing response: evidence for facilitation, latent inhibition, and perceptual learning. Q. J. Exp. Psychol. B 46, 271–288 (1993). [PubMed: 8210452]
34. Radulovic J, Kammermeier J & Spiess J Relationship between Fos production and classical fear conditioning: effects of novelty, latent inhibition, and unconditioned stimulus preexposure. J. Neurosci. 18, 7452–7461 (1998). [PubMed: 9736664]
35. Do-Monte FH, Quinones-Laracuente K & Quirk GJ A temporal shift in the circuits mediating retrieval of fear memory. Nature 519, 460–463 (2015). [PubMed: 25600268]
36. Frankland PW, Bontempi B, Talton LE, Kaczmarek L & Silva AJ The involvement of the anterior cingulate cortex in remote contextual fear memory. Science 304, 881–883 (2004). [PubMed: 15131309]
37. Hall J, Thomas KL & Everitt BJ Cellular imaging of zif268 expression in the hippocampus and amygdala during contextual and cued fear memory retrieval: selective activation of hippocampal CA1 neurons during the recall of contextual memories. J. Neurosci. 21, 2186–2193 (2001). [PubMed: 11245703]
38. Xu W & Sudhof TC A neural circuit for memory specificity and generalization. Science 339, 1290–1295 (2013). [PubMed: 23493706]
39. Melzer S et al. Long-range-projecting GABAergic neurons modulate inhibition in hippocampus and entorhinal cortex. Science 335, 1506–1510 (2012). [PubMed: 22442486]
40. Takacs VT, Szonyi A, Freund TF, Nyiri G & Gulyas AI Quantitative ultrastructural analysis of basket and axo-axonic cell terminals in the mouse hippocampus. Brain Struct. Funct. 220, 919–940 (2015). [PubMed: 24407853]
41. Toth K & Freund TF Calbindin D28k-containing nonpyramidal cells in the rat hippocampus: their immunoreactivity for GABA and projection to the medial septum. Neuroscience 49, 793–805 (1992). [PubMed: 1279455]

42. Jinno S et al. Neuronal diversity in GABAergic long-range projections from the hippocampus. J. Neurosci. 27, 8790–8804 (2007). [PubMed: 17699661]
43. Buzsaki G & Chrobak JJ Temporal structure in spatially organized neuronal ensembles: a role for interneuronal networks. Curr. Opin. Neurobiol. 5, 504–510 (1995). [PubMed: 7488853]
44. Lux V, Atucha E, Kitsukawa T & Sauvage MM Imaging a memory trace over half a life-time in the medial temporal lobe reveals a time-limited role of CA3 neurons in retrieval. eLife 5, e11862 (2016). [PubMed: 26880561]
45. Guo N et al. Dentate granule cell recruitment of feedforward inhibition governs engram maintenance and remote memory generalization. Nat. Med. 24, 438–449 (2018). [PubMed: 29529016]
46. Ruediger S et al. Learning-related feedforward inhibitory connectivity growth required for memory precision. Nature 473, 514–518 (2011). [PubMed: 21532590]
47. Kim JJ & Fanselow MS Modality-specific retrograde amnesia of fear. Science 256, 675–677 (1992). [PubMed: 1585183]
48. Goshen I et al. Dynamics of retrieval strategies for remote memories. Cell 147, 678–689 (2011). [PubMed: 22019004]
49. Kitamura T et al. Engrams and circuits crucial for systems consolidation of a memory. Science 356, 73–78 (2017). [PubMed: 28386011]
50. Moscovitch M, Cabeza R, Winocur G & Nadel L Episodic memory and beyond: the hippocampus and neocortex in transformation. Annu. Rev. Psychol. 67, 105–134 (2016). [PubMed: 26726963]
51. Paxinos G & Franklin KBJ The Mouse Brain in Stereotaxic Coordinates (Academic Press, 2012).
52. Richards BA et al. Patterns across multiple memories are identified over time. Nat. Neurosci. 17, 981–986 (2014). [PubMed: 24880213]
53. Rashid AJ et al. Competition between engrams influences fear memory formation and recall. Science 353, 383–387 (2016). [PubMed: 27463673]
54. Wang SH, Teixeira CM, Wheeler AL & Frankland PW The precision of remote context memories does not require the hippocampus. Nat. Neurosci. 12, 253–255 (2009). [PubMed: 19182794]
55. Arruda-Carvalho M et al. Conditional deletion of α-CaMKII impairs integration of adult-generated granule cells into dentate gyrus circuits and hippocampus-dependent learning. J. Neurosci. 34, 11919–11928 (2014). [PubMed: 25186740]
56. Restivo L, Niibori Y, Mercaldo V, Josselyn SA & Frankland PW Development of adult-generated cell connectivity with excitatory and inhibitory cell populations in the hippocampus. J. Neurosci. 35, 10600–10612 (2015). [PubMed: 26203153]
57. Chen S et al. A hypothalamic novelty signal modulates hippocampal memory. Nature 586, 270–274 (2020). [PubMed: 32999460]

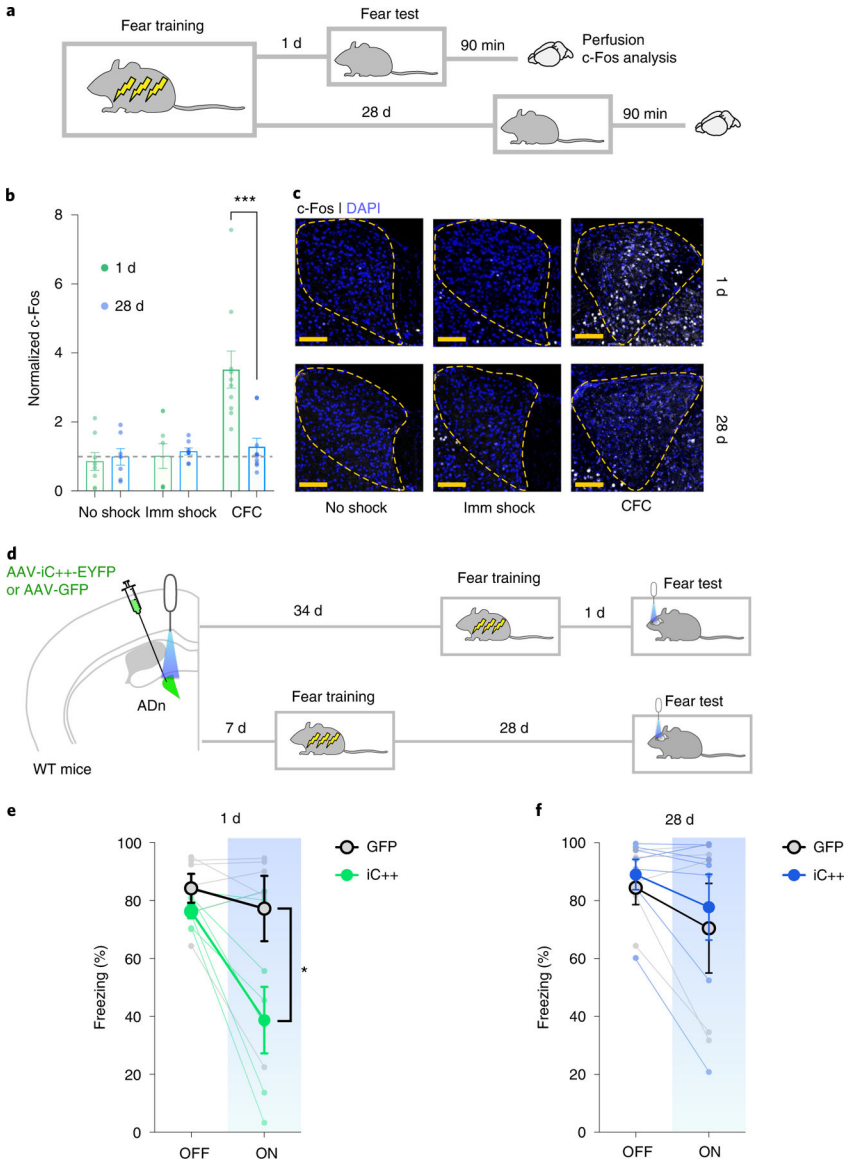

Fig. 1 |. ADn activity is necessary for recall of recently acquired contextual fear memory.

a, Mice were trained in contextual fear conditioning and tested 1 or 28 d later. At 90 min after the test, mice were killed and their brains processed for c-Fos expression in ADn. **b**, Expression of c-Fos in ADn (normalized to mean expression level in home-cage control mice $n = 16$) in no shock (1 d $n = 8$; 28 d $n = 7$; two-sided Mann–Whitney test, $P = 0.62$; 1 d versus one, one-sample two-sided Wilcoxon signed-rank test, $P = 0.55$; 28 d versus one, one-sample two-sided Wilcoxon signed-rank test, $P > 0.99$) or immediate shock (Imm shock; 1 d $n = 8$; 28 d $n = 8$; two-sided Mann–Whitney test, $P = 0.62$; 1 d versus one, one-sample two-sided Wilcoxon signed-rank test, $P > 0.99$; 28 d versus one, one-sample two-sided Wilcoxon signed-rank test, $P = 0.38$) control groups was similar at 1 and 28 d, and not different from home-cage controls. However, expression of c-Fos in ADn in mice trained in contextual fear conditioning (CFC) was higher in mice tested at 1 d, in comparison with home-cage controls, but not in mice tested 28 d post-training (1 d $n =$

10; 28 d $n = 10$; two-sided Mann–Whitney test, $P = 0.0003$; 1 d versus one, one-sample two-sided Wilcoxon signed-rank test, $P = 0.002$; 28 d versus one, one-sample two-sided Wilcoxon signed-rank test, $P = 0.70$). **c**, Representative images showing expression of c-Fos in ADn in mice following no shock (repeated in $n = 8$ (1 d); $n = 7$ (28 d)), immediate shock (repeated in $n = 8$ (1 d); $n = 8$ (28 d)) or contextual fear conditioning and testing at 1- and 28-d time-points (repeated in $n = 10$ (1 d); $n = 10$ (28 d); scale bar, 100 μm). **d**, WT mice were micro-infused with AAV-iC++-EYFP or the control virus AAV-GFP in the ADn, and optical fibers were implanted above the ADn. During fear memory testing at 1 or 28 d post-training, ADn was optogenetically inactivated. **e**, At the 1-d test, iC++- and GFP-infused mice froze equally during the light-OFF epoch (3-min duration), but iC++-infused mice showed reduced freezing in comparison with GFP-infused mice during the light-ON epoch (3-min duration) (iC++ $n = 6$; GFP $n = 6$; two-sided Mann–Whitney test iC++ versus GFP, $P = 0.004$; OFF: two-sided Wilcoxon signed-rank test iC++ versus GFP, $P = 0.18$; ON: two-sided Wilcoxon signed-rank test iC++ versus GFP, $P = 0.03$). **f**, At the 28-d test, iC++- and GFP-infused mice froze equally during light-OFF and light-ON epochs (iC++ $n = 5$; GFP $n = 7$; two-sided Mann–Whitney test iC++ versus GFP, $P = 0.47$; OFF: two-sided Wilcoxon signed-rank test iC++ versus GFP, $P = 0.43$; ON: two-sided Wilcoxon signed-rank test iC++ versus GFP, $P = 0.88$). Data are individual mouse or mean ± s.e.m. ($^{*}P < 0.05$, $^{***}P < 0.001$).

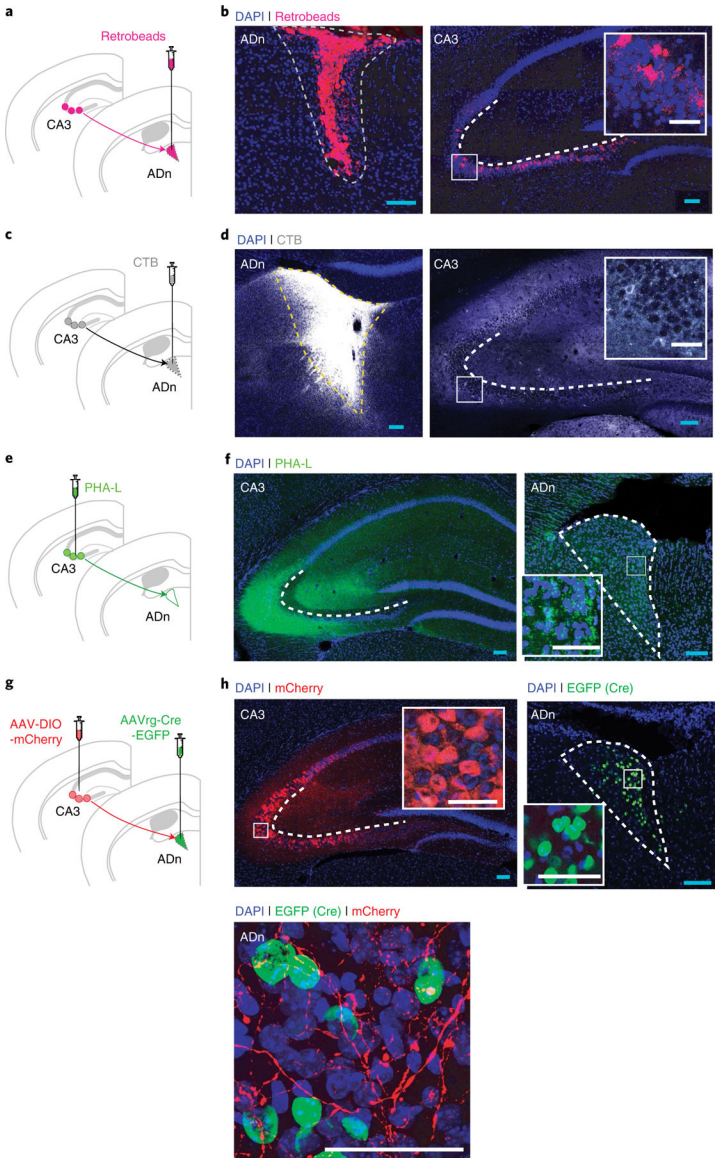

Fig. 2 |. Identification of anatomical projections to the ADn.

a,**b**, WT mice were micro-infused with retrograde tracer Retrobeads ($n = 3$) in the ADn and retrograde-labeled neurons in CA3 were visualized. **c**,**d**, WT mice were micro-infused with retrograde tracer CTB (n = 3) in the ADn and retrograde-labeled neurons in CA3 were visualized. **e**,**f**, For anterograde labeling, WT mice were micro-infused with anterograde tracer PHA-L ($n = 4$) in the CA3 and anterograde labeling was visualized in ADn. **g**,**h**, To visualize specifically CA3–ADn projections, WT mice were micro-infused with AAV-DIO-mCherry bilaterally in CA3 and AAVrg-Cre-EGFP unilaterally in ADn. CA3–ADn ($mCherry^+$) projections were visualized in ADn ($n = 4$; blue scale bars, 100 μm; white scale bars, 50 μm).

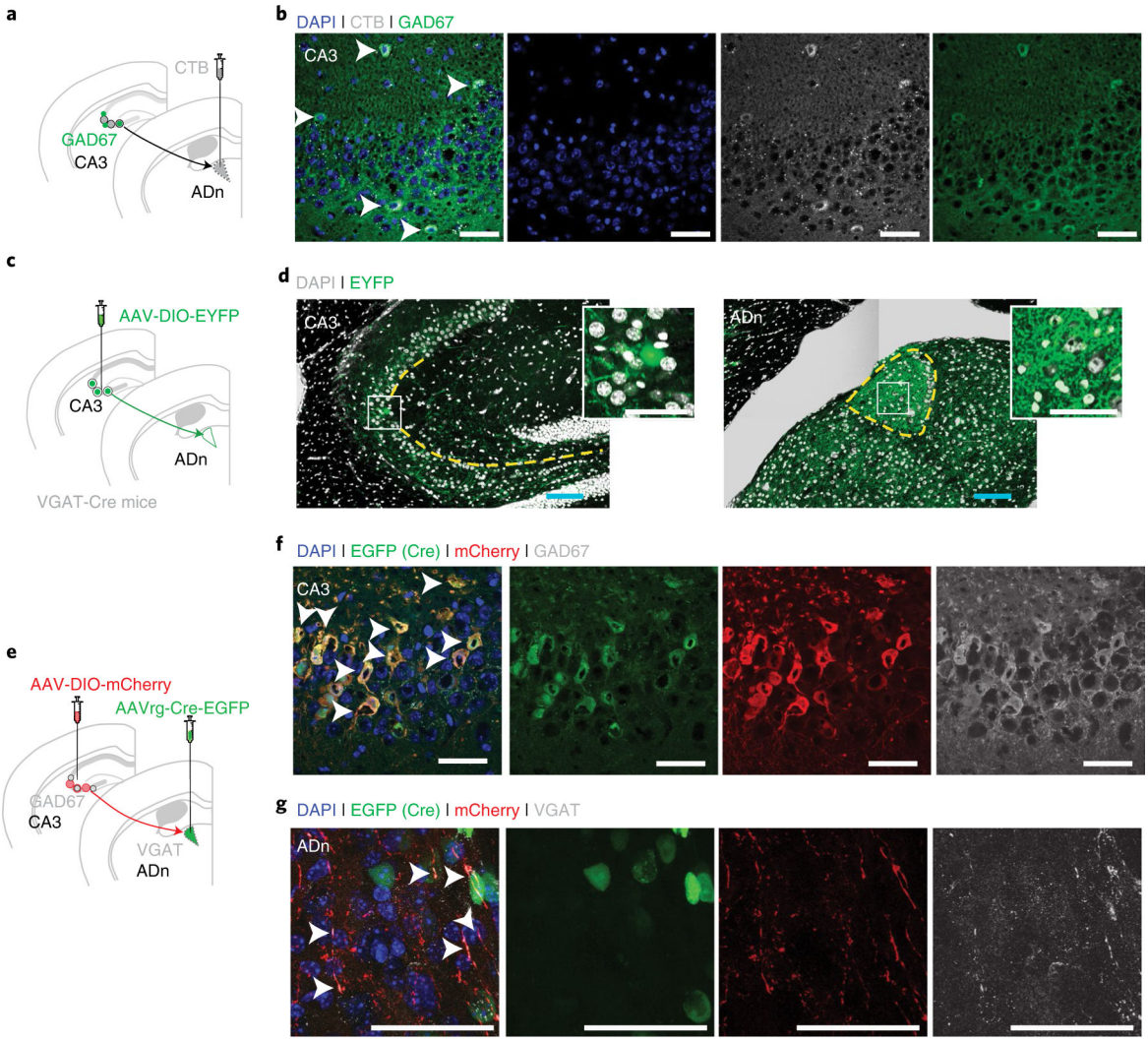

Fig. 3 |. Identification of inhibitory projections to the ADn.

a,**b**, WT mice were micro-infused with CTB ($n = 3$) in the ADn, and retrograde-labeled neurons in CA3 were visualized. Sections were costained with the inhibitory cell marker GAD67. Numerous CTB^+ and $GAD67^+$ colocalized cells were visualized in CA3 (white arrows). **c**,**d**, To identify inhibitory projections to the ADn, VGAT-Cre mice were micro-infused with AAV-DIO-EYFP in CA3 ($n = 3$). Strong terminal projections were visualized in the ADn. **e**–**g**, To visualize specifically CA3–ADn projections and examine whether they are inhibitory, WT mice were micro-infused with AAV-DIO-mCherry bilaterally in CA3 and AAVrg-Cre-EGFP unilaterally in ADn, and sections were costained with (**f**) GAD67 (CA3) or (**g**) VGAT (ADn) ($n = 4$). Numerous inhibitory CA3–ADn projection neurons in CA3 ($mCherry^+$ and $GAD67^+$, white arrows) and projections in ADn ($mCherry^+$ and $VGAT^+$, white arrows) were visualized (blue scale bars, 100 μm; white scale bars, 50 μm).

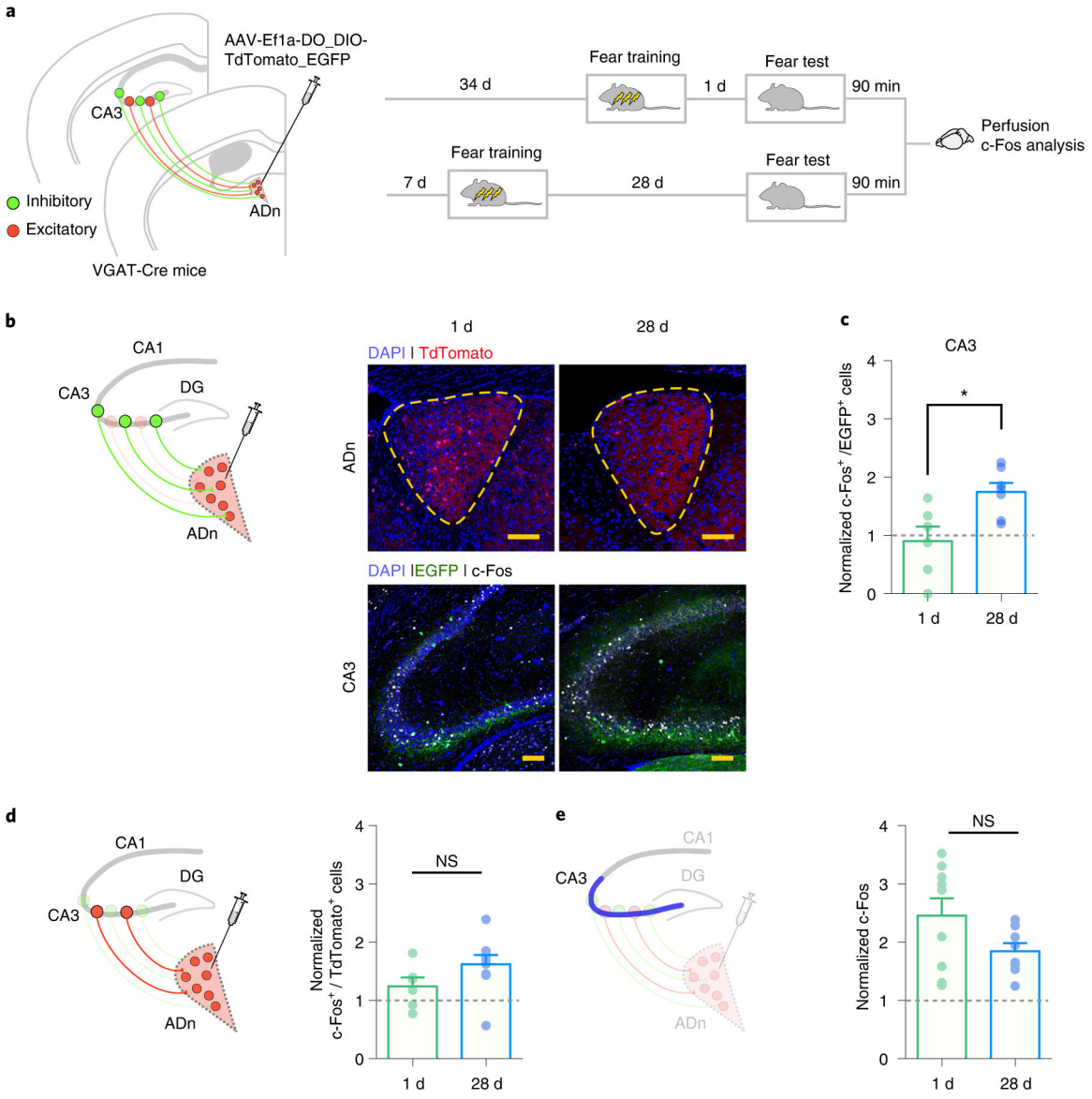

Fig. 4 |. CA3 inhibitory cells projecting to the ADn become more active at the remote time-point post-training.

a, VGAT-Cre mice were micro-infused with AAV-Ef1a-DO_DIO-TdTomato_EGFP in ADn to retrogradely label inhibitory (EGFP$^+$) and excitatory (TdTomato$^+$) cells that project to the ADn. After viral infusion, mice were then trained in contextual fear conditioning and tested 1 or 28 d post-training. At 90 min after the test, mice were killed and their brains processed to analyze c-Fos expression in CA3. **b**, Representative images showing viral infusion site in the ADn, retrogradely labeled inhibitory cells in CA3 and expression of c-Fos in both regions, at 1 and 28-d time-points (repeated in $n = 6$ (1 d); $n = 7$ (28 d); scale bar, 100 μm). **c**, Mice tested at 28 d post-training showed higher colocalization of EYFP$^+$ and c-Fos$^+$ cells in CA3, in comparison with mice tested at 1 d post-training (colocalization of EYFP$^+$ and c-Fos$^+$ cells, normalized to mean colocalization level in home-cage control mice ($n = 4$), adjusted for multiple-comparisons with Bonferroni–Dunn method; 1 d $n = 6$; 28 d $n = 7$; two-sided t-tests $t_{11} = 2.98$, $P = 0.038$). **d**, Mice tested at 1 or 28 d post-training showed

similar levels of colocalization of TdTomato$^+$ and c-Fos$^+$ cells in CA3 (colocalization of EYFP$^+$ and c-Fos$^+$ cells, normalized to mean colocalization level in home-cage control mice (n = 3), adjusted for multiple-comparisons with Bonferroni–Dunn method; 1 d n = 6; 28 d n = 9; two-sided t-tests t_{13} = 1.62, P = 0.39). **e**, Mice tested at 1 or 28 d post-training showed similar levels of total c-Fos$^+$ cells in CA3 (total c-Fos$^+$ cells normalized to mean c-Fos levels in home-cage control mice (n = 7), adjusted for multiple-comparisons with Bonferroni–Dunn method; 1 d n = 9; 28 d n = 8; two-sided t-tests t_{15} = 1.77, P = 0.29). Data are mean ± s.e.m. (NS, not significant; *P < 0.05).

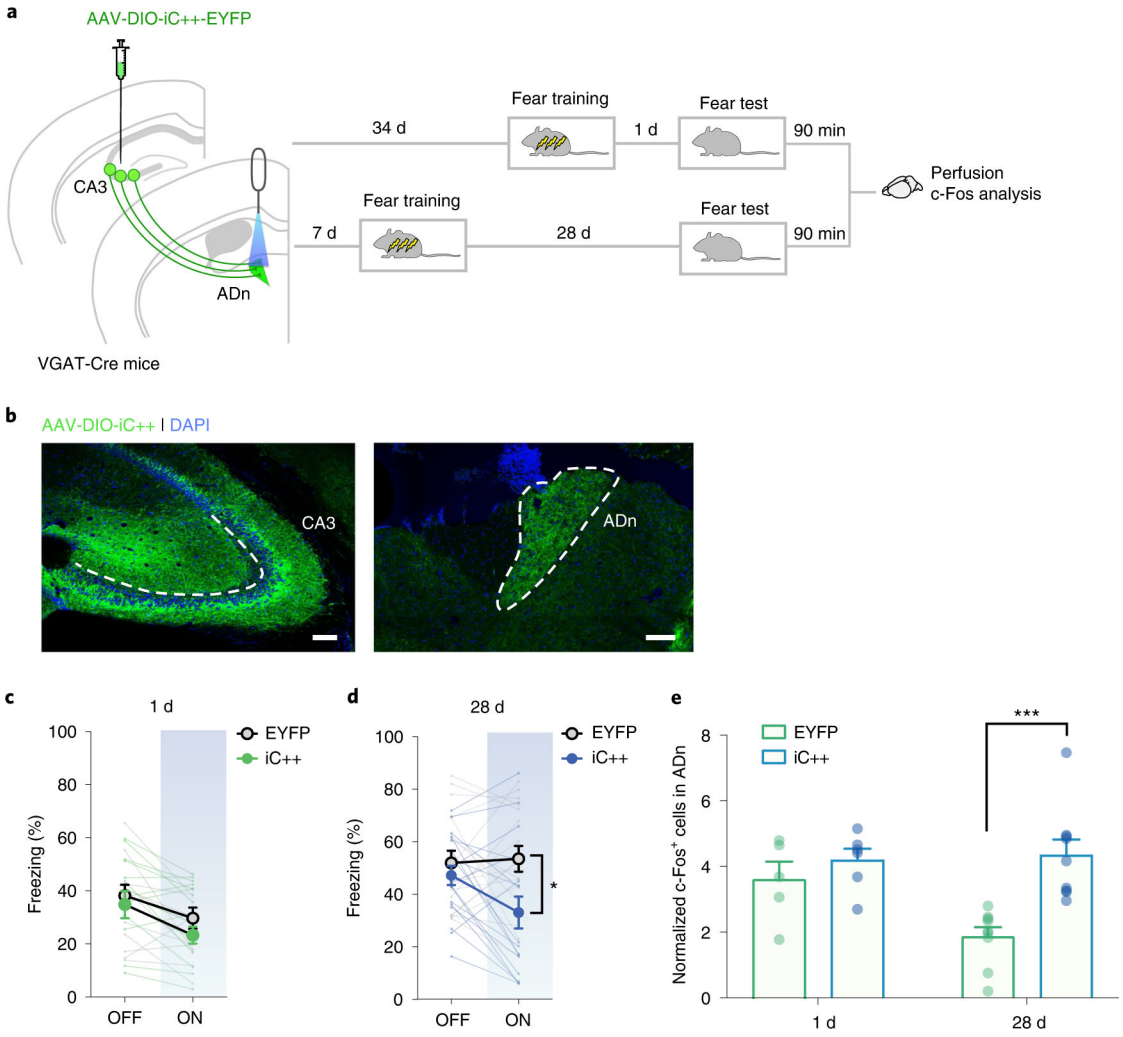

Fig. 5 |. cA3 inhibitory cells projecting to the ADn are necessary for the recall of remote memory. **a**, VGAT-Cre mice were micro-infused with AAV-DIO-iC++-EYFP or AAV-DIO-EYFP virus in CA3 and optical fibers were implanted in the ADn, to optogenetically inhibit the CA3–ADn projection during fear memory test, at 1 or 28 d post-training. At 90 min after the test, mice were killed and their brains processed to analyze c-Fos expression in ADn. **b**, Representative images showing viral infection in CA3 and projections in ADn (repeated in $n = 14$ (iC++); $n = 11$ (EYFP); scale bar, 100 μm). **c**, At 1-d test, iC++- and EYFP-infused mice froze equally during light-OFF and light-ON epochs (iC++ $n = 14$; EYFP $n = 11$; two-way repeated-measures ANOVA iC++ versus EYFP × light-OFF versus light-ON; interaction, $F_{1,46} = 0.13$, $P = 0.72$; light-OFF versus light-ON, $F_{1,46} = 5.71$, $P = 0.02$; iC++ versus EYFP, $F_{1,46} = 1.35$, $P = 0.25$). **d**, At 28-d test, iC++- and EYFP-infused mice froze equally during light-OFF epoch (3-min duration), but iC++-infused mice showed reduced freezing in comparison with EYFP-infused mice during light-ON epoch (3-min duration) (iC++ $n = 18$; EYFP $n = 17$; two-sided Mann–Whitney test iC++ versus EYFP, $P = 0.03$; OFF: two-sided Wilcoxon signed-rank test iC++ versus EYFP, $P = 0.68$; ON: two-sided Wilcoxon signed-rank test iC++ versus EYFP, $P = 0.014$). **e**, At 1 d, iC++-infused mice showed an equivalent level of c-Fos expression in the ADn (normalized to mean

expression level in home-cage control mice ($n = 16$)), in comparison with EYFP-infused control mice. But at 28 d, iC++-infused mice showed an elevated level of c-Fos expression in the ADn, in comparison with controls (1 d: iC++ $n = 6$; EYFP $n = 5$; 28 d: iC++ $n = 9$; EYFP $n = 9$; two-way ANOVA iC++ versus EYFP × 1 d versus 28 d; interaction, $F_{1,25} = 4.77$, $P = 0.039$; 1 d versus 28 d, $F_{1,25} = 3.27$, $P = 0.083$; iC++ versus EYFP, $F_{1,25} = 12.62$, $P = 0.0015$; post hoc Bonferroni's test, 1-d iC++ versus EYFP $P = 0.79$, 28-d iC++ versus EYFP $P = 0.0002$). Data are individual mouse, or mean ± s.e.m. (*$P < 0.05$, ***$P < 0.001$).